

Alma Mater Studiorum – Università di Bologna

DOTTORATO DI RICERCA IN

Bioingegneria

Ciclo XXIX

Settore Concorsuale: 05/E1- BIOCHIMICA GENERALE

Settore Scientifico Disciplinare: BIO/10 – BIOCHIMICA

TITOLO TESI

**"INVESTIGATING THE MECHANOBIOLOGY OF
CANCER CELL-ECM INTERACTION: THE IMPACT
OF SUBSTRATE STIFFNESS IN BREAST CANCER
PROGRESSION"**

Presentata da: Chiara Liverani

Coordinatore Dottorato

Prof. Daniele Vigo

Supervisore

Prof. Emanuele Giordano

Co-Supervisore

Dott. Toni Ibrahim

Esame finale anno 2018

TABLE OF CONTENTS

1. Abstract.....	5
2. Introduction.....	8
2.1 Breast cancer.....	8
2.2 The extracellular matrix	9
2.3 The role of extracellular matrix in cancer.....	10
2.4 Extracellular collagen and its modification.....	12
2.5 Collagen remodeling in breast cancer	13
2.6 The role of the matrix-modifying enzyme LOX	14
2.7 Three-dimensional (3D) in vitro models to study cancer	17
2.8 Cancer cell response to matrix stiffness in 3D models.....	19
2.9 Determination of the mechanical properties of soft tissue biomaterials	21
2.10 Dynamic Mechanical Analysis.....	23
2.11 Atomic Force Microscopy.....	25
2.12 Translational impact of these studies.....	28
3. Aims.....	31
4. Material and methods.....	33
4.1 Experimental <i>in vitro</i> model.....	33
4.2 Synthesis of the porous collagen scaffolds.....	34

4.3 Cell seeding and culture.....	35
4.4 Cell quantification.....	36
4.5 Histological analysis.....	36
4.6 LOX inhibition.....	37
4.7 Scaffold decellularization.....	37
4.8 Development of a low-force mechanical testing device.....	37
4.9 Mechanical testing.....	39
4.9.1 Low-force testing device.....	39
4.9.2 Dynamic Mechanical Analysis (DMA)	39
4.9.3 Atomic Force Microscopy (AFM)	40
4.10 Microscopy analysis.....	42
4.11 Quantitative Real-Time Reverse Transcription-PCR (qRT-PCR).....	42
4.12 MTT assay.....	43
4.13 Drug testing.....	43
4.14 Xenograft study.....	44
4.15 Collagen staining.....	44
4.16 Statistical analysis.....	45
5. Results.....	46
5.1 Collagen remodeling in breast xenograft tumors.....	46
5.2 Collagen scaffold macro and micro properties	49
5.3 Phenotypes and behavior of breast cancer cells on the collagen matrix.....	51
5.4 Assessment of the low-force testing device repeatability.....	59
5.5 Alteration of the compressive stiffness of collagen scaffolds by invasive breast cancer cells.....	60
5.6 Dynamic Mechanical analysis of collagen scaffolds.....	63

5.7 Collagen scaffold remodeling by breast cancer cells.....	67
5.8 LOX inhibition impairs MDA-MB-231 ability to increase collagen stiffness.....	72
5.9 Atomic Force Microscopy analysis of single collagen fibers.....	74
6. Discussion.....	78
7. Conclusions and future perspectives.....	88
8. References.....	90
9. Acknowledgments	101
10. List of Publications and Conference Proceedings.....	103

1. Abstract

Rationale

The extracellular matrix (ECM) properties can be modified in multiple pathological processes either as a cause or as a result of the disease pathogenesis. In cancer, the loss of tissue homeostasis and mechanoreciprocity are considered one of the disease hallmarks. In particular, breast cancer has been defined as a disease of altered mechanobiology. It has been shown that an ECM gene signature can stratify breast cancer patients into subclasses that predict outcome. Increased breast tumor density in mammography has proven to be significantly correlated with reduced progression-free survival in metastatic patients. Studies on the tumor mechanobiology are thus expected to provide an insight into the disease pathogenesis as well as potentially useful biomarkers.

Type I collagen is among the major determinants of breast ECM structural and tensile properties, and the collagen modifications during tumor evolution drive a number of disease-related processes that favor cancer progression and invasion. Here we have applied a porous type I collagen-based three-dimensional (3D) scaffold to study how breast cancer cells interact and alter extracellular collagen. Combining this culturing technique with different methodologies to characterize the structural and mechanical properties of collagen-based scaffolds we assessed the modifications induced by tumor cells on the micro- and macro- characteristic of extracellular collagen and on its compressive stiffness.

Materials and methods

The human breast cancer cell lines MCF7 and MDA-MB-231 were cultured for 10 days on porous collagen scaffolds. The two cell lines belong to breast tumor subtypes

characterized by different clinical aggressiveness and distinct *in vivo* ECM characteristics. MCF7 belong to the luminal A subtype and have a weak *in vitro* invasiveness, while MDA-MB-231 are basal-like breast cancer cells that are associated with a highly aggressive behavior. At the end of the culturing time, we characterized the cell morphological and molecular phenotypes and their drug sensitiveness. We next tested, the changes induced by cancer cells in the stiffness property of the scaffold, and in its structural micro- and macro- architecture. Mechanical testing was conducted both with an in-house built low-force compressive device and by Dynamic Mechanical Analysis. The stiffness of single collagen fibers was also assessed by Atomic Force Microscopy. We next used orthotopic xenotransplantation of the two cell lines to evaluate the collagen content and the degree of macroscopic collagen remodeling in *in vivo* breast tumors.

Results

When cultured on collagen scaffolds, the two cell lines generated coherent tissue-like structures. MCF7 displayed an epithelial morphology with a tightly cohesive cobblestone appearance and high levels of E-cadherin expression, while MDA-MB-231 showed a mesenchymal phenotype with lower cell-to-cell contact, a spindly appearance and high vimentin expression. MDA-MB-231, which belongs to the aggressive basal-like subtype, increased scaffold stiffness from 46.9 ± 2.7 kPa, to 57.9 ± 3.6 kPa, and overexpressed the matrix-modifying enzyme, lysyl oxidase (LOX), whereas luminal A MCF-7 cells did not significantly alter the mechanical characteristics of extracellular collagen. These data were obtained either using an in-house built mechanical testing device, and a Dynamic Mechanical Analysis, a standard technique to measure the properties of biomaterials.

The phenotype observed *in vitro* replicates the behavior of *in vivo* tumors generated by MDA-MB-231, characterized by higher collagen content and LOX levels than MCF-7.

When the activity of LOX was blocked, MDA-MB-231 were unable to increase the scaffold stiffness: scaffold compressive modulus increased by only 8.9%, in contrast to the increase observed without LOX inhibition (23%).

No significant changes were observed between the Young's modulus of fibers taken from control scaffolds, which was 1.08 ± 0.24 GPa, compared to the Young's modulus of fibers taken from scaffolds decellularized after the culture with MDA-MB-231, which was $1.1 \text{ GPa} \pm 0.05$.

Conclusions

Overall this work provides evidence that invasive, mesenchymal-like breast cancer cells produce high levels of the collagen crosslinking enzyme LOX, and are able to increase the stiffness of extracellular type I collagen and to alter its structural characteristics. Measurements of the compressive modulus of these soft synthetic extracellular matrices were carried out using a prototypal mechanical testing instrument originally designed and developed. A causal relationship between LOX expression and the ability of cancer cells to alter the stiffness of extracellular collagen was also provided.

Our model offers a relevant *in vitro* tool to reproduce and investigate the biomechanical interplay subsisting between cancer cells and the surrounding ECM and its impact on the tumor phenotype and behavior.

2. Introduction

2.1 Breast cancer

Breast cancer is the most prevalent cancer diagnosed in women worldwide, and is the second leading cause of cancer death in women (Desantis et al., 2013 and Siegel et al., 2016). It is now the most common cancer both in developed and developing regions. Breast cancer ranks as the fifth cause of death from cancer overall (Ferlay J et al., 2012). The majority of breast cancers diagnosed are ductal invasive carcinomas that arise from luminal or basal epithelial cells. Breast cancer can be classified into four categories based on microarray gene expression profile analysis: luminal A and luminal B subtypes, characterized by the expression of the Estrogen Receptor (ER) and the Progesterone Receptor (PGR); the HER2-positive subtype, characterized by the overexpression of the human epidermal growth factor receptor 2 (HER2); and the basal-like subtype (Basal A and Basal B) characterized by triple negativity for ER and PGR expression and for HER2 overexpression (Sorlie et al., 2001). Expression of estrogen receptor (ER), progesterone receptor (PR), and HER2 receptor is used to determine the primary breast tumor subtype, the prognosis, and the targeted therapeutic regimen. Estrogen receptor (ER) and progesterone receptors (PR) are treated as predictive and prognostic markers (as per National Academy of Clinical Biochemistry guidelines). ER- α and PR should be measured in all patients with breast cancer and have clinical application. The presence of ER is an important discriminating factor: ER-positive tumors are associated with better prognosis, longer relapse-free survival, and improved overall survival compared to ER-negative tumors (Zhang et al., 2014 and Hoch et al., 1999). A number of targeted hormonal therapy are available for these patients. HER2-positive breast tumors show more aggressive features, but the treatment options have advanced through the use of monoclonal

antibodies to block HER2 activity (Dent et al., 2013). HER2 should be measured in all patients with invasive breast cancer. The primary purpose of measuring HER2 is to select patients with breast cancer that may be treated with trastuzumab.

Ten to twenty percent of all invasive breast cancers diagnosed are classified as triple negative breast cancer (TNBC), a subtype characterized by lack of expression of ER or PR, and lack of HER2 overexpression. TNBCs typically are diagnosed at higher tumor stage and grade, show an aggressive biology and are associated with poor prognosis. Treatment options for TNBC patients are restricted to the use of cytotoxic chemotherapies, since these tumors do not respond to anti-hormonal therapy (Tomaio et al., 2015). Even if TNBC patients usually respond to chemotherapy, they have shorter relapse-free survival (Carey et al., 2007 and Hudis et al. 2011). TNBC tumors are also more likely to develop resistance to chemotherapies and present with distant recurrence and visceral metastases (Carey et al., Hudis et al. and Anders et al.). Consequently, in order to advance the development of targeted therapeutics in TNBC, a better understanding of the underlying molecular mechanisms distinguishing TNBC from other breast cancer subtypes is critical.

2.2 The extracellular matrix

The extracellular matrix (ECM) is the non-cellular component of all tissues and organs, that provides essential physical scaffolding for the cells, and regulates crucial biochemical and mechanical cues that are required for tissue morphogenesis, differentiation and homeostasis. The importance of the ECM is clearly demonstrated by the wide range of diseases that arise from genetic abnormalities in ECM proteins (Jarvelainen H et al., 2009). Essentially, the ECM is composed of two main classes of macromolecules: proteoglycans (PGs) and fibrous proteins. Each tissue has an ECM with a unique composition and topology that is generated during tissue development through a dynamic

interplay between the various cellular components (e.g. epithelial, fibroblast, adipocyte, endothelial elements) and the evolving cellular and protein microenvironment.

Cell adhesion to the ECM is mediated by ECM receptors, such as integrins, discoidin domain receptors and syndecans (Frantz C et al., 2010). Adhesion mediates cytoskeletal coupling to the ECM and is involved in cell migration through the ECM (Schmidt S. and Friedl P., 2010). The ECM generates the biochemical and mechanical properties of each organ, such as its tensile and compressive strength and its elasticity. In addition, the ECM directs essential morphological organization and physiological function by binding growth factors (GFs) and interacting with cell-surface receptors to modulate signal transduction and gene transcription (Hynes RO, 2009).

The ECM is a highly dynamic structure that is constantly being remodeled, either enzymatically or non-enzymatically, and its molecular components are subjected to a number of modifications. The physical, topological, and biochemical composition of the ECM is not only tissue-specific, but is also markedly heterogeneous (Frantz C et al., 2010). ECM biochemical and mechanical properties in a given tissue can change from one physiological state to another. Also the composition and the architecture of the ECM, its interactions with the cellular constituents, and its post-translational modifications can vary extremely in a pathological conditions (for examples in aged tissue, wounded or fibrotic tissue and tumors). This ECM remodeling, in turn, cause functional consequences on cellular behaviors including altered GF sensitivity elicited by changes in ECM tension (Frantz C et al., 2010).

2.3 The role of extracellular matrix in cancer

The ECM has a vital role in the regulation of various biological pathways contributing to development, tissue homeostasis and diseases (Bonnans et al., 2014). ECM is involved in

a number of different biological processes as the maintenance of tissue polarity, the induction or blockade of cell migration, the creation of molecule concentration gradients and the exertion of direct intracellular signals (**Figure 1**).

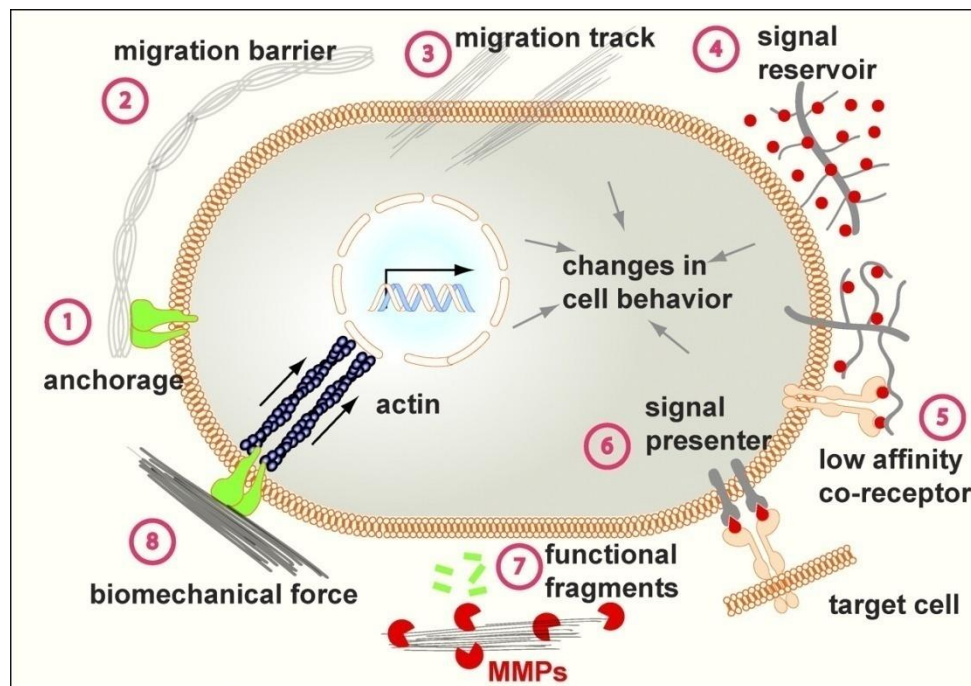


Figure 1: schematic representation of the role of the ECM in different cellular processes (Pengfei et al., 2012).

In particular, forces are essential for normal tissue-specific organization, in which they regulate cell survival, growth and migration, coordinating tissue development and function.

ECM properties can be modified in multiple pathological processes either as a cause or as a result of the disease pathogenesis (Bonnans et al., 2014). Cancer is no longer merely considered as a disease of tumor cells: the imbalance of the tumor microenvironment also appears to play a crucial role. ECM, as the most abundant component in the tumor

microenvironment, can regulate cancer cell behavior and affect key tumor processes (Pengfei et al., 2012). Loss of tissue homeostasis and mechanoreciprocity are considered a hallmark of cancer.

In particular, breast cancer has been defined as a disease of altered mechanobiology: matrix density, structure and stiffness, together with interstitial fluid pressure and flow, change during tumor evolution (Dvorak et al., 2011). As an example, the collagen matrix of breast cancer stroma is significantly stiffer and more linearized than in normal tissue, due to a progressive enzymatic crosslinking mediated by cancer cells. Linearized collagen fibers can, in turn, increase growth factor-dependent cell migration (Levental et al., 2009). Two primary mechanisms are involved in migration of cancer cells: the cell physical rearrangement linked to the epithelial to mesenchymal transition (EMT) (Mierke et al., 2011 and Hoffman et al., 2011), and the reorientation of collagen by traction forces and by enzymatic cleavage (Wolf et al., 2007 and Gonzalez et al., 2010). Both can be regulated by tissue tension. Increased matrix cross-linking and ECM protein deposition or parallel reorientation of collagen can stiffen tissue locally and drive migration. Altered mechanical signaling can also affect cell survival, division and differentiation (Du Fort et al., 2011; Engler et al., 2006 and Janmey et al., 2011). ECM remodeling is thus capable of affecting a number of tumor processes such as invasion, progression (Levental et al., 2009), and metastasis initiation (Provenzano et al., 2006).

2.4 Extracellular collagen and its modification

Collagens comprise a large family of triple helical proteins and are the most abundant protein in human tissues, accounting for one-third of total proteins. There are now at least 29 genetically distinct types of collagen identified, that are encoded by at least 44 genes that can be divided into several subgroups, depending on the molecular structure and

assembly mode (Hulmes, 2008). Fibril-forming collagens comprise the largest subgroup, including types I, II, III, V, XI, XXIV and XXVII. Fibrillar type I collagen is the most abundant type providing most tissues and organs with form, stability and connectivity. In addition to the structural functions, type I and other collagens also function as ligands for specific cell receptors, such as integrins, discoidin domain receptors, glycoprotein VI and the mannose receptor family etc., to control cellular activities and extracellular matrix remodeling (Leitinger, 2011). One of the most important factors for the structural and biomechanical functions of type I collagen fibrils are the post-translational modifications of peptidyl lysine residues. These modifications are highly regulated processes that can take place either inside or outside the cell. In the cell, the peptidyl lysine residues can be hydroxylated both in the helical and non-helical (telopeptide) domains of the molecule. Specific hydroxylysine residues in the helical domain can then be glycosylated with the addition of galactose, some of which can be further glycosylated with the addition of glucose. Specific enzymes catalyse each of these sequential and domain-specific lysine modifications. Outside the cell, an enzymatic oxidative deamination occurs to the telopeptidyl lysine and hydroxylysine residues, producing reactive aldehydic residues. The aldehydes then initiate a series of chemical condensation reactions to form extensive covalent intra- and inter-molecular cross-links, which are critical for the biomechanical functions of the collagen fibrils (Yamauchi, 2008).

2.5 Collagen remodeling in breast cancer

Increased deposition of collagens I, III and IV and enhanced collagen matrix cross-linking are among the ECM structural changes that occur during tumor progression (Zhu et al., 1995; Lesniak et al., 2010 and Fang et al., 2014). Increased deposition and remodeling creates a reorganized microenvironment with significant impacts on tumor cell biology

including gene expression, cell differentiation, proliferation, migration and responses to treatments (Paszek et al., 2005).

Breast cancer is a typical example of these changes. Collagen is the major component of the breast connective tissue and is a key determinant of its tensile properties (Roeder et al., 2002) and of the macroscopic deformability of mammary tumors (Fenner et al., 2014) that are characterized by high collagen content and remodeling (Schedin et al., 2011). Clinicians have long recognized the connection between breast density and breast cancer risk (Wolfe, 1976). Collagen surrounding normal epithelial structures in breast tissue is typically curly and smooth. However, parallel with tumor development, collagen progressively thickens, linearizes and stiffens fostering cell migration into ECM. Intravital imaging shows that breast cancer cells and leukocytes migrate rapidly along collagen fibers (Wyckoff et al., 2007). Cancer cells might exploit these remodeled stiff collagens as invasion "highways".

2.6 The role of the matrix-modifying enzyme LOX

Extracellular collagen remodeling is predominantly catalyzed by enzymes such as lysyl oxidase (LOX) (Xiao and Ge, 2012). There are five lysine or hydroxylysine residues in the telopeptide domains of type I collagen, two in the C- and three in the N- telopeptide. These five lysine/hydroxylysine residues can be oxidatively deaminated by the copper (Cu²⁺)-dependent amine oxidase LOX to form the respective aldehydes which initiates a series of condensation reactions to form covalent intra- and inter-molecular cross-links (**Figure 2**) (Yamauchi and Sricholpech, 2012).

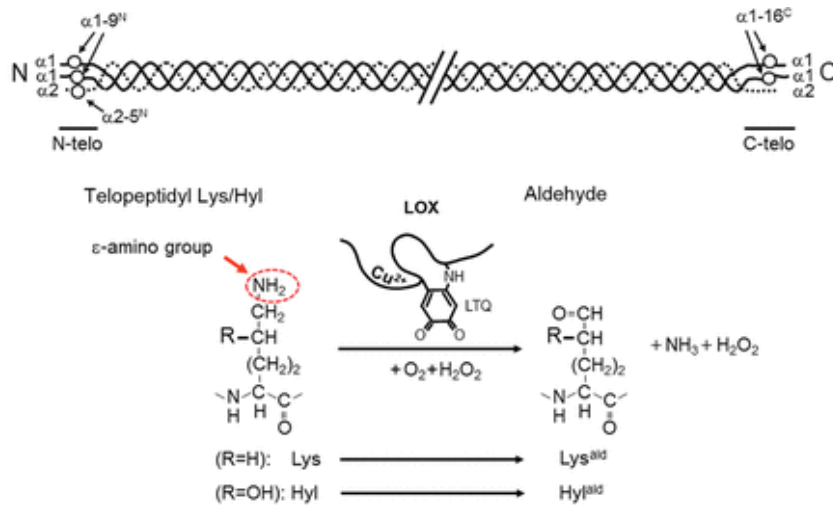


Figure 2. Lysine modifications in the telopeptide domains of type I collagen (Yamauchi and Sricholpech, 2012).

LOX has been found to be synthesized in response to hypoxic conditions: hypoxia promote HIF-1- α mediated endogenous LOX gene expression. Subsequently, the collagen maturation occurs through the extracellular modification of collagen fibers by LOX, resulting in the formation of covalent cross-links (Makris et al., 2014) (**Figure 3**).

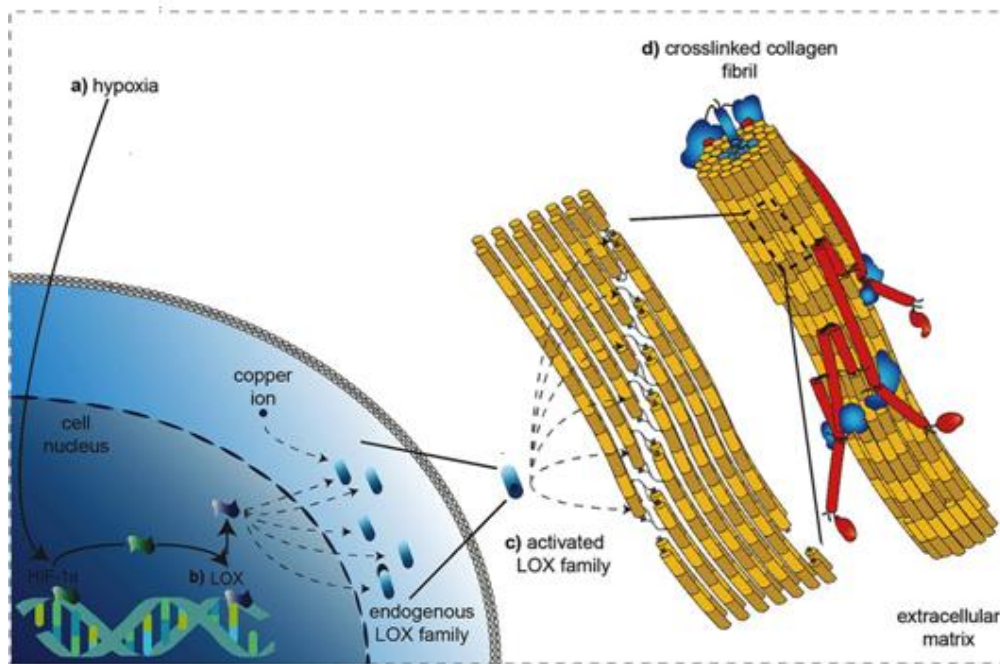


Figure 3. Mechanistic description of HIF-1–mediated LOX transcription and subsequent collagen cross-linking that enhance the biomechanical properties of collagen-rich tissues (Makris et al., 2014).

In tumors, LOX can be synthesized by either stromal cells during early stages of carcinogenesis, or tumor cells during late stages of tumor progression. LOX, secreted by hypoxic tumor cells, crosslink collagens and elastin, thereby increasing insoluble matrix deposition and tissue stiffness (Erler et al., 2009).

This enzyme have demonstrated a crucial role in breast cancer progression and metastatic spread. LOX is essential in driving tumor cells escape from primary site, extravasation and growth at secondary sites during metastasis (Erler et al., 2006 and Erler et al., 2009). It is reported that LOX can also be disseminated into distal target organs via circulation to create pre-metastatic niche both at lung (Erler et al., 2009) and bone sites (Cox et al., 2015), as also evidenced by a consistent correlation between increased LOX expression and higher cancer metastasis risk (Erler et al., 2006). Finally, increased LOX expression is

associated with early stromal reaction in breast cancer, and reactive fibrosis at the invasive front of infiltrating tumors also releases high levels of LOX (Erler and Giaccia, 2006).

2.7 Three-dimensional (3D) *in vitro* models to study cancer

In vitro research offers several experimental methods and models to investigate the tumor mechanobiology (Carey et al., 2012). However, studies examining the relationship between ECM mechanics and cell phenotype have been hampered by limitations in the experimental approaches used to manipulate the biophysical properties of the ECM. The systems predominantly applied are mechanically tunable two-dimensional (2D) polymer hydrogels conjugated with ECM ligands (Tse et al., 2010; Young et al., 2011). These 2D substrates, unfortunately, fail to model the heterogeneous and three-dimensional (3D) structure of native tissue. For this reason, a number of innovative 3D systems have recently been developed and applied to investigate how cancer cells interact with the ECM, or to address the impact of mechanical signaling in diverse tumor phenotypes and behaviors in a more physiological context (Cassereau et al., 2015; Paszek et al., 2005 and Wozniak et al., 2012). By employing 3D hydrogel substrates, Paszek and colleagues found that matrix compliance differs dramatically between 2D and 3D cultures, and between normal versus tumoral tissue *in vivo*. In this work the faithful recapitulation of tissue morphogenesis is favored by matrix conditions with an elastic modulus that corresponds with that of normal tissues *in vivo*. By examining the relationship between tissue rigidity and tumor behavior, Paszek and colleagues showed that tissue rigidity is linked to matrix stiffening and affects Rho GTPase-dependent cytoskeletal tension. They also found that matrix stiffness and cytoskeletal tension cooperate to modulate tissue behavior: matrix stiffness influences tissue growth and morphogenesis by modulating cell contractility, while tensional homeostasis appears to be necessary for normal tissue behavior. These

findings provided a new perspective on the role of the tissue microenvironment in tumorigenesis, providing new possible therapeutic targets (Paszek et al., 2005).

However, the use of hydrogel still presents some limitations, including the failure to control the pore size, and the gel inconsistencies. On the other hand, synthetic polymer scaffolds allow for the fine-tuning of ECM mechanical properties, but fail to recapitulate the architecture and composition of a natural ECM, not enabling cells to interact and remodel the scaffold matrix (Miroshnikova et al., 2011; Miller et al., 2010). 3D biomimetic matrices represent the ideal systems to efficiently recapitulate tissue dimensionality and the biomechanical and physical cues of tumor ECM (Infanger et al., 2013). Collagen-based scaffolds provide an efficient tool to mimic the ECM of soft tissues for *in vitro* research. These scaffold ideally show: i) high biocompatibility to allow cells to attach and proliferate; ii) a highly porous structure to allow cell and nutrient infiltration; iii) similar mechanical properties to the native tissue (Lamhamedi-Cherradi et al., 2014). Provenzano and colleagues, employed 3D collagen matrices that closely resemble the ECM architectures observed *in vivo*. They showed that utilizing *in vivo*-mimicking ECM conditions facilitates the acquisition of physiologically relevant information, while permitting manipulation of the system, and they used this matrix assays for studying contact guidance *in vitro* (Provenzano et al., 2010). Casserau and colleagues developed a novel tension bioreactor system that employs a native collagen I hydrogel and permits consistent manipulation of ECM stiffness in the absence of modifications to the structure, composition, or pore size of the gel. This system permitted precise mechanical tuning of collagen stiffness, while maintaining constant composition and pore size. Using this system Casserau and colleagues demonstrated that increasing ECM stiffness potentiates tumor cell migration, validating the use of this model to study malignant transformation and the invasive and migratory phenotype of tumor cells (Cassereau et al., 2015).

In conclusion natural and synthetic matrices can be used to recapitulate the interstitial ECM in *in vitro* culture with the aim to study tissue behavior or to deconstruct and analyze how specific ECM parameters (stiffness, fiber orientation, ligand presentation, dimensionality) provoke specific cellular behaviors (**Figure 4**).

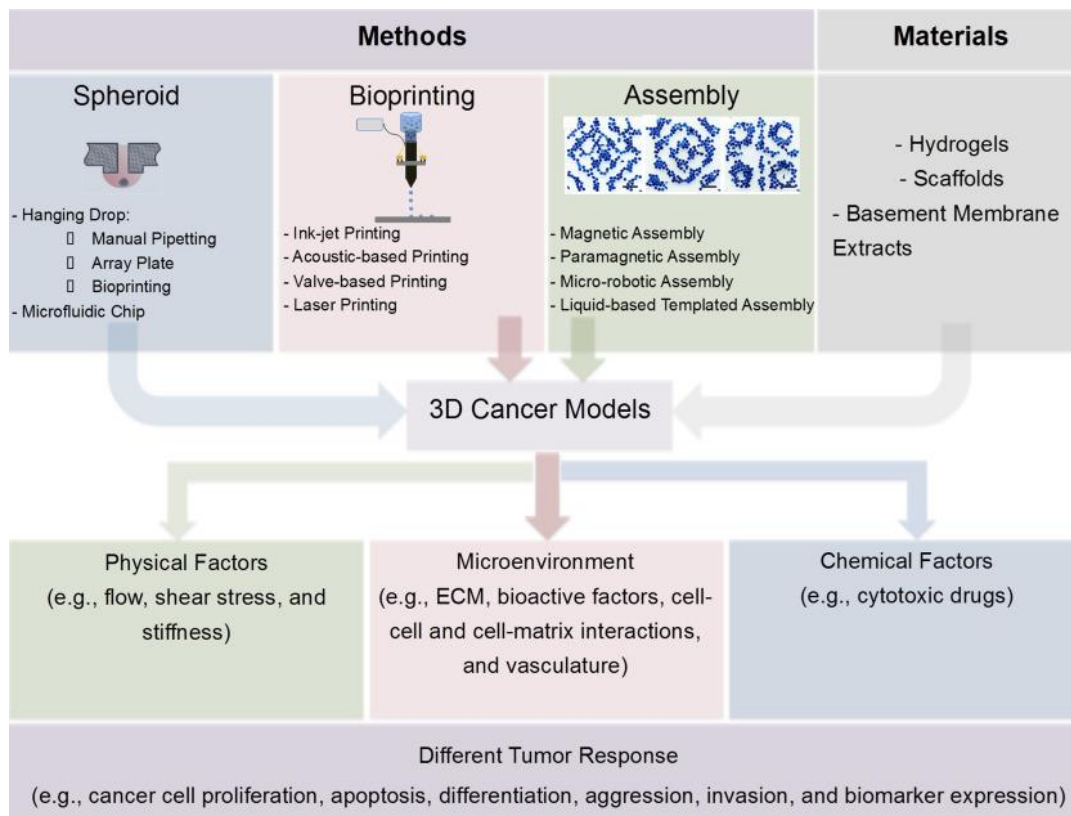


Figure 4. Schematic of the *in vitro* models presently used to generate 3D cancer cultures, with different methods and materials and control of physical and biochemical factors (Asghar et al., 2015).

2.8 Cancer cell response to matrix stiffness in 3D models

Matrix stiffness is an important parameter when studying the cellular response of cancer cells in 3D microenvironment (Chauhan VP et al., 2014). The matrix stiffness of different organs and tissues can be quantified by the Young's modulus (E) that can be soft as the brain tissue (ranging from 250 to 500 Pa) or rigid as the bone tissue (ranging from 1 to 25

GPa). The cellular response in microenvironments with different degrees of ECM mechanical stiffness is different. The matrix stiffness of solid tumors changes during the course of cancer metastasis and progression (Paszek et al., 2005). For instance, the microenvironment of breast tumor show a matrix with a high degree of stiffness (4000 Pa) compared to the healthy breast tissue (200 Pa) (Butcher et al., 2009) (**Figure 5**).

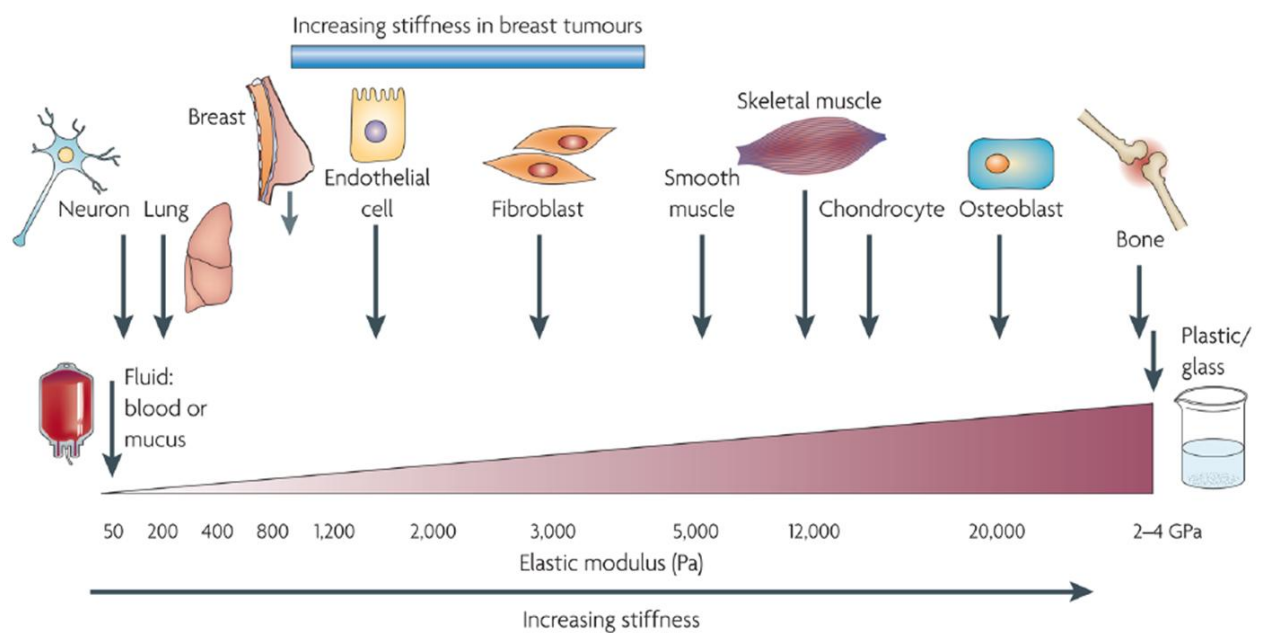


Figure 5. Schematic representation of the stiffness properties of different human cells and tissues, and of the increasing stiffness observed in breast tumors (Butcher et al., 2009).

One of the most effective protein hydrogels that has been used to investigate cancer cell response to 3D matrices with different stiffness is collagen hydrogels, as previously described (Paszek et al., 2005). Stromal collagen deposition and crosslinking can define the stiffness of the tumor microenvironment and consequently can alter the cancer cell migration through the ECM (Carey et al., 2012). In another report, a polyacrylamide

hydrogel substrate with varying stiffness was used to demonstrate that cells migrated from the soft substrate to the stiffer substrate (Levental et al., 2009). In another investigation, metastatic cancer cells were characterized by measuring the traction forces applied to 2D and 3D matrices by cancer cells on these substrates (Kraning-Rush et al., 2012). Breast, lung, and prostate cancer cells showed significantly stronger traction forces on the substrate at the late stage of the cancer disease compared to the normal healthy cells. Further, these results showed that cancer cells created stronger contractile forces on matrices with higher stiffness. The degrees of the traction and contraction forces generated by cancer cells are determined by the chemical and mechanical properties of the tumor microenvironment.

2.9 Determination of the mechanical properties of soft tissue biomaterials

The determination of mechanical properties of *in vitro* constructed ECM, as hydrogels or scaffolds, has becoming an important challenge for studying cell responses in these in 3D environments. Unlike hard tissue matrices, the mechanical properties of soft tissues can be challenging to be characterized. They usually can tolerate minimum stress, making it difficult to obtain precise measurement. Several experimental methods including three point bending, lateral and axial fiber vibration measurement, and direct axial tension tests have been exploited in recent years to characterize the mechanical properties of nanofibers (Edmondson et al, 2009). As an example, Florczyk and colleagues used dynamic mechanical compression to determine the stiffness of porous chytosan-hyaluronic acid matrices to recreate a scaffold with a Young's modulus similar to that of the brain tissue and study human glioblastoma cells (Florczyk et al., 2013).

Other reported also the development of an in-house built instrument to measure the stiffness of small soft tissue samples. Fenner and colleagues developed a system to measure the nonlinear elastic behavior of soft tissues, using a cylindrical piston of known length and volume to indent tumor samples at steps of a known length (**Figure 6**), and recording changes in force for each successive step size that the cylindrical piston was applied to the specimen. The piston force, when knowing the degree of surface displacement, provided the nonlinear geometric stiffness characteristic for the given tumors. Using this system they were able to find an inverse correlation between the bulk modulus of freshly resected breast tumors generated by cancer cells xenotransplantation in murine models and the development of subsequent local recurrence and metastasis. In particular, the authors found that mice with compliant tumors were developing more frequent and larger local recurrences, and more extensive metastases than mice with relatively stiff tumors (Fenner et al., 2014).



Figure 6. Photo of the piston compression device system used by Fenner and colleagues to measure the bulk moduli of ex vivo breast tumors (Fenner et al., 2014)

Another recently developed solution is to determine matrices elastic modulus through nanoindentation (Zhu et al., 2011). Nanoindentation has been applied for characterizing

many soft materials' mechanical properties (Doubé et al., 2010). In nanoindentation test, small loads can be used with an Atomic Force Microscope (AFM) (Barone et al., 2010). AFM can measure forces at the nN level (Clifford and Seah, 2006 and Darling et al., 2007) allowing measurement with a size-scale comparable to the cellular one, for a better understanding of the cell-substrate stiffness interaction. For example, Cavo and colleagues used AFM to measure the stiffness of an alginate hydrogel where breast cancer cells were cultured, demonstrating that stiffness directly influences cells fate (Cavo et al., 2016).

Rheological testing has also been applied to study the mechanical properties of soft biological materials (Elango et al., 2016 and Yang et al., 2009). Although the storage moduli from rheological measurements is much different from tangent stiffness and, in rheological test, the movement of the interstitial fluid play a significant role in determining the overall mechanical properties of the samples (Xu et al., 2011).

Combining the recently developed 3D culture systems with devices that can measure the mechanical characteristics of small tissue, gel or scaffold samples might shed new light on the relation between the stiffness properties of ECM and tumor cells and its influence on pathological cancer processes. The use of different techniques to measure the diverse mechanical properties that tissues exhibit under specific loading conditions can further improve our understanding on the cancer mechanobiology.

2.10 Dynamic Mechanical Analysis

Dynamic mechanical analysis (DMA) is a non-destructive technique widely used for the mechanical characterization of polymer-based systems, which is getting increasing importance in biomaterial research. Basically, it allows to characterize the viscoelastic properties of materials in a wide temperature and frequency ranges, by monitoring the

sample's response upon an imposed controlled cyclic load (with the corresponding development of stresses) or strain (Mano et al., 2002). The instrumentation of a DMA consists of a displacement sensor, such as a linear variable differential transformer (LVDT), a temperature control system or furnace, a force generator, a drive shaft support and guidance system to act as a guide for the force from the motor to the sample, and sample clamps in order to hold the sample being tested (**Figure 7**).

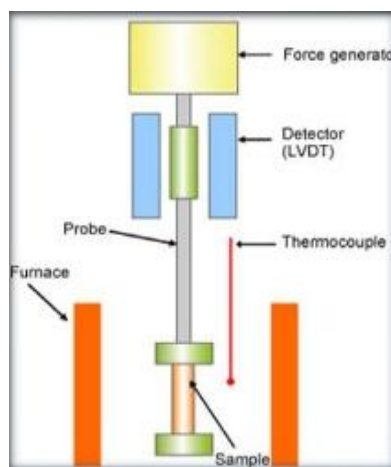


Figure 7. Schematic of the main component of a dynamic mechanical analysis instrument.

The samples is clamped into a frame and it is heated by the furnace. In the furnace the stress is applied from the force generator via a probe. The stress is applied as a sinusoidal force, to make the strain amplitude constant. The deformation of the sample is then detected. Mechanical properties such as elasticity or viscosity are derived from the stress applied and the strain, and plotted as a function of temperature or time. Several DMA equipments are now available, enabling studies in different mechanical configurations such as in tensile, flexural, compression or shear modes. Such studies are particularly relevant if the tests are performed at physiologically meaningful conditions, i.e., with the specimens completely incubated in solutions at 37 °C (Ghosh et al., 2008).

2.11 Atomic Force Microscopy

In order to improve the applicability of soft biomaterials, as collagen scaffolds, a characterization of their structure and properties at a nanoscale level is required. This characterization can be performed by Atomic Force Microscopy (AFM) (Stylianou and Yova, 2013). AFM is a scanning probe microscope that records interactions between a probe and the sample surface. This technique has been introduced in 1980s, by Binnig and colleagues (Binnig et al., 1986), and has now become a fundamental method in surface and biomedical sciences.

The AFM apparatus usually consists of a laser beam deflection system (optical lever) where a laser beam is reflected from the back of a cantilever (on which a very sharp tip is mounted to come into contact with a sample surface) and onto a position-sensitive detector (Stylianou A, 2017) (**Figure 8**).

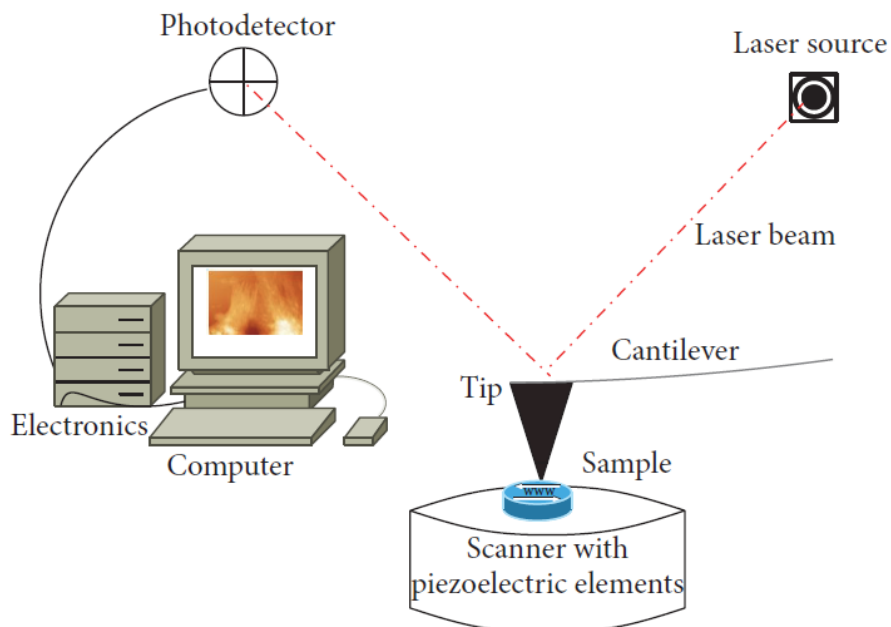


Figure 8. Schematic of an AFM apparatus consisting of a probe (cantilever and tip), a laser source, a scanner, a photodetector, the electronics, and a computer (Stylianou A, 2017).

The AFM gathers information with the probe, which is the tip mounted on the cantilever. The probe scans the sample surface and measures the atomic forces among probe sample surfaces. The accurate movement of the tip over the surface of a sample under the tip, depending on the system, is achieved with piezoelectric elements. The measurement of the tip deflection is obtained via a laser beam and then transferred to the system's electronics which form 3D images of the samples and/or assess other sample's properties, such as stiffness, roughness or adhesion. The AFM can perform force spectroscopy of force volume for measuring mechanical properties of the samples: indentation-force curves are formed and fitted using mathematical expressions to calculate values that are needed for measuring the sample's Young modulus and for creating material's properties maps (e.g., Young's modulus maps). Various theoretical and empirical models can be used to analyse force-displacement curves: the Hertz theory (Hertz, 1981; Kurland et al., 2012), the Johnson-Kindall-Roberts (JKR) model (Johnson et al., 1971) or the Derjaguin-Müller-Toporov (DMT) model (Derjaguin et al., 1975). Recently, Bruker develop a new operating mode of AFM, called Peak Force Tapping. It provides high resolution images at a relatively high speed. When the tip is distant from the surface there is little or no force on the tip. As it approach the sample surface the cantilever is pulled down by attractive forces such as van der Waals, electrostatics or capillary forces. Then the tip touches the surface and stays on it until the Z position reaches its lowest position while the force is increasing. A constant force at this point is maintained by adjusting the extension of Z piezo through a feedback loop. After that the probe starts to withdraw and the force decreases until its minimum: at this point the surface forces of adhesion are determined. Finally, the tip leaves the surface and only long range forces affect it, and when the tip-sample separation is at its maximum there is a very small or zero force. Dependence of the force against the

Z-position can be compared with force-displacement curves that have usually been used in measuring mechanical properties of a sample. When the force curve is complete it is then analyzed to obtain the properties of the sample and the information is sent to one of the image data channel. Different material properties can be extracted, as elastic modulus, adhesion, energy dissipation and maximum deformation. The results are presented as maps of material properties in user-defined false colours (Kolářová et al., 2012).

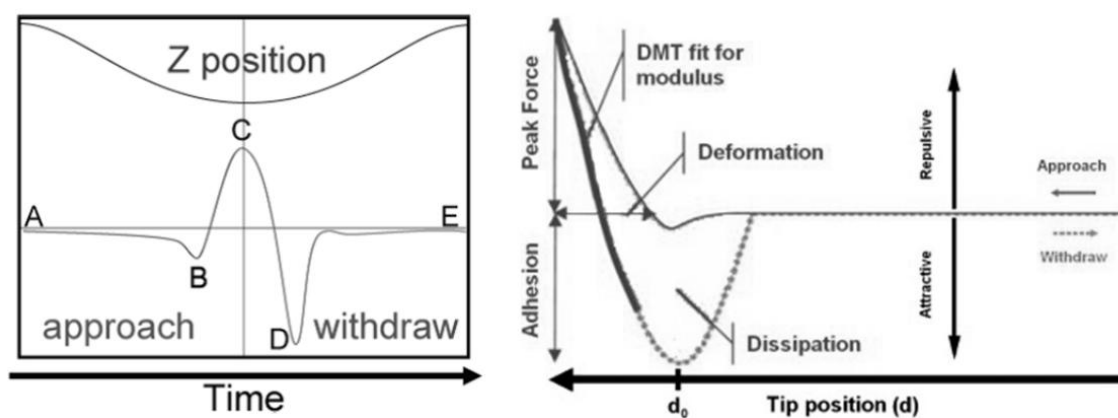


Figure 9. Schematic representation of the indentation steps (left), and of the mechanical informations (right) of the peak force tapping operating model of AFM (Kolářová et al., 2012).

Compared to other techniques AFM has unique advantages, in particular over other microscopy techniques, such as Scanning or Transmission Electron Microscopy (SEM and TEM) and optical microscopy. First of all, AFM provides topological information at the nanoscale level that other microscopes cannot measure. Moreover, AFM can perform the characterization of the mechanical properties of samples at a nanoscale level, offering thus a combination of qualitative and quantitative information. Furthermore, AFM possesses the ability to perform nanoscale imaging/characterization without the need for presence of

vacuum conditions or any special treatment of the specimen, such as sample labeling or surface coating (Allison et al., 2010). AFM can be used for investigating a wide range of collagen-based structures, from collagen molecules to separated fibrils and fibers and collagen-based nanobiomaterials as well (Cisneros et al., 2007). The AFM characterization can be performed without destroying the fibrillar structure of collagen. As an example Zhu and colleagues successfully applied AFM nanoindentation in a liquid fashion to characterize the stiffness and the elastic modulus of collagen–chitosan hydrogel (Zhu et al., 2011).

2.12 Translation impact of these studies

Investigations into breast tumor biomechanics provided a new insight into the disease pathogenesis, leading to the identification of clinically useful biomarkers. It has been shown that an ECM gene signature can stratify breast cancer patients into subclasses that predict outcome (Plodinec et al., 2012 and Bergamaschi et al., 2008). Bergamaschi and colleagues proved that primary breast tumors can be stratified upon ECM composition and that this classification provides relevant information on the biology of breast carcinomas, further supporting the hypothesis that clinical outcome is strongly related to stromal characteristics (Bergamaschi et al., 2008).

Furthermore, molecular profile analyses carried out in other breast cancer cohorts as well as other tumor types, indicated that matrix molecules are present in expression signatures that classify disease progression (Perou et al., 2000; Sorlie et al., 2001; Van't Veer and Weigelt, 2003; Sotiriou et al., 2003; Teschendorff et al., 2007 and Mintz et al., 2005). Increased breast tumor density in mammography has proven to be significantly correlated with reduced progression-free survival in metastatic patients (Elsamany et al., 2014) and

to be an excellent predictor of response to tamoxifen in the preventive setting (Cuzick et al., 2011). With an observational study on breast cancer patients with metastatic disease, Elsamany and colleagues demonstrated that progression-free survival (PFS) was correlated with breast density. PFS, stratified by different prognostic factors, was assessed in low- compared to high-density patients. Among the enrolled patients, median PFS in low-density patients was significantly better than those with high density. Breast density assessed at the time of diagnosis was significantly correlated with PFS of metastatic breast cancer patients, while survival outcome was improved in specific patients' subgroups with low breast density (Elsamany et al., 2014).

Finally, Cuzick and colleagues conducted a nested case-control study within the first International Breast Cancer Intervention Study, a randomized prevention trial of tamoxifen vs. placebo. Mammographic breast density was assessed visually and expressed as a percentage of the total breast area in 5% increments. Case subjects were 123 women diagnosed with breast cancer at or after their first follow-up mammogram, which took place 12-18 months after trial entry. Control subjects were 942 women without breast cancer. In the tamoxifen arm, 46% of women had 10% or greater reduction in breast density at their 12- to 18-month mammogram. Compared with all women in the placebo group, women in the tamoxifen group who experienced 10% or greater reduction in breast density had 63% reduction in breast cancer risk, whereas those who took tamoxifen but experienced less than 10% reduction in breast density had no risk reduction. In the placebo arm, there was no statistically significant difference in breast cancer risk between subjects who experienced less than 10% reduction in mammographic density and subjects who experienced a greater reduction. The 12- to 18-month change in mammographic breast density thus emerged as an excellent predictor of response to tamoxifen in the preventive setting (Cuzick et al., 2011).

All these examples show how the study of the tumor mechanobiology can provide new possible disease biomarkers or therapeutic targets to help clinicians in the diagnosis, prognosis and treatment of breast cancer patients.

3. Aims

In the present study we used an *in vitro* 3D cell culture model, based on porous type I collagen scaffolds, to investigate the ability of breast cancer cells to produce alterations in the structural and mechanical characteristics of extracellular collagen. This biomimetic matrix, providing a physiological 3D network, constitutes the model of choice to reproduce *in vitro* the cell-ECM interactions. We studied and applied different mechanical testing techniques and microscopy characterizations to assess the changes induced by cancer cells on the micro- and macro-structural properties of the collagen scaffolds, on the material median compressive stiffness and on the Young's modulus of single collagen fibers.

Specifically we:

- i. evaluated the phenotypes and behavior of two subtypes of breast cancer, characterized by different clinical aggressiveness, when cultured within the collagen scaffolds;
- ii. developed a prototype low-force instrument to measure the compressive properties of the collagen scaffolds;
- iii. evaluated the modifications induced by breast cancer cells on the compression-dependent viscoelastic properties of the scaffolds;
- iv. evaluated the modifications induced by breast cancer cells on the micro properties of single collagen fibers;
- v. evaluated the modifications induced by breast cancer cells on the micro/macro-structures and protein composition of the scaffolds;
- vi. fabricated collagen scaffolds tuned to recreate distinct stiffness properties.

The overall aim was to demonstrate whether this 3D *in vitro* model might offer a valid and informative tool to recapitulate and investigate the biomechanical interaction that occurs between breast cancer cells and the surrounding ECM, focusing on the ability of invasive cancer cells to modify the structural and stiffness properties of extracellular collagen.

4. Materials and Methods

4.1 Experimental *in vitro* model

Two different human breast cancer cell lines, MCF-7 and MDA-MB-231, were cultured for 10 days on 3D porous collagen scaffolds. MCF-7 cells belong to the luminal A subtype of breast cancer (ER positive) and are associated with weak *in vitro* invasiveness, whereas MDA-MB-231 belong to the basal-like subtype (triple negative breast cancer TNBC) and are associated with an invasive behavior (Holliday et al., 2011) and the ability to colonize different sites (*e.g.* bone, liver, lung and brain) after intravenous injection (Kang et al., 2003). From the clinical standpoint the luminal A subtype is often connected to indolent disease and a better prognosis, while the basal-like subtype is connected to high-grade and aggressive disease. At the end of the culture time, the phenotypes of the two cell lines were characterized by morphological and molecular analyses.

The scaffold samples were decellularized and their macro- and micro- mechanical and structural properties were tested to assess the modifications induced in the collagen matrix by either cell line (Liverani et al., 2017) (**Figure 10**).

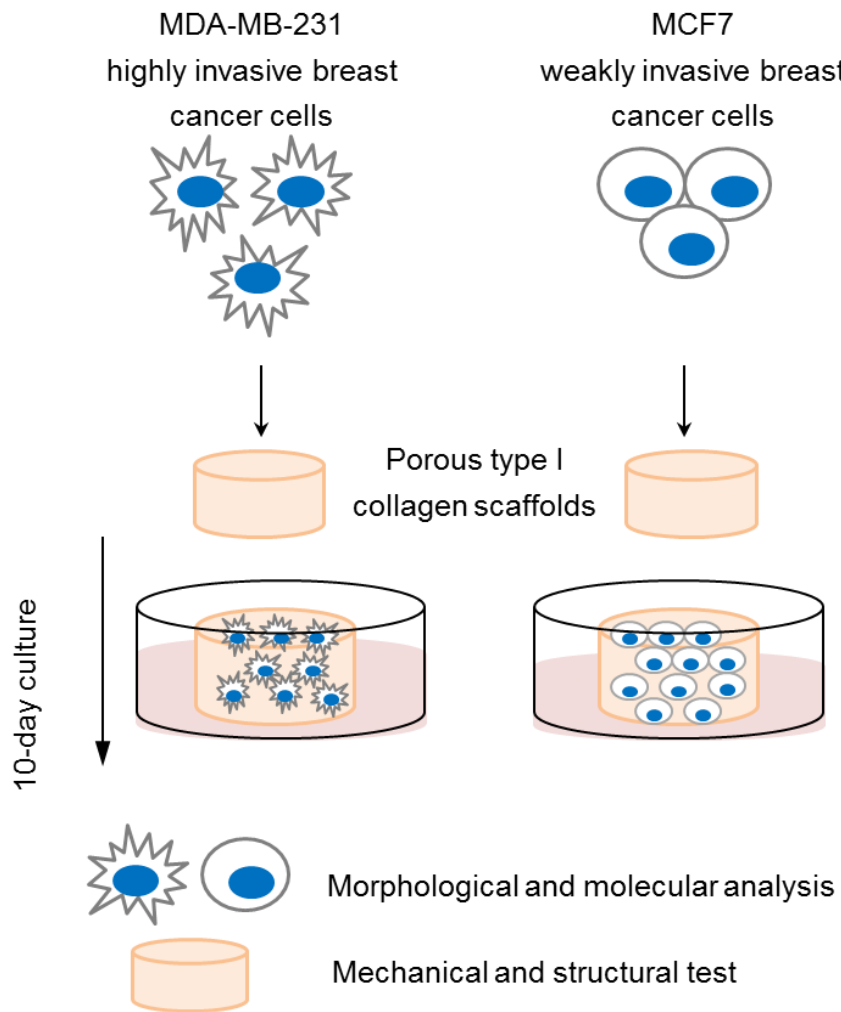


Figure 10. Two human breast cancer cell lines, MCF-7 and MDA-MB-231, characterized by a diverse aggressive behavior, were cultured for 10 days on porous collagen-based 3D scaffolds. At the end of the culture time, cells were characterized for morphological and molecular phenotypes and the mechanical and structural properties of the scaffolds were analyzed (Liverani et al., 2017).

4.2 Synthesis of the porous collagen scaffolds

All chemicals were purchased from Sigma Aldrich (USA). The scaffolds were synthesized from type I bovine collagen as described elsewhere (Minardi et al., 2014). Briefly, a 1 wt% collagen suspension in acetate buffer (pH 3.5) was prepared. The collagen was then precipitated at pH 5.5 with NaOH 1M. The collagen was then washed three times with

deionized water and then crosslinked in an aqueous solution of 1,4-butanediol diglycidyl ether (BDDGE) (2.5 mM), for 24 h. This cross-linking step is essential to determine the stiffness of the collagen matrix: higher concentrations of the crosslinking reagent (BDDGE) can generate scaffolds with increasing stiffness properties. Finally, the collagen was washed three times and casted in Teflon molds (9 mm in diameter) and freeze dried through an optimized freezing and heating ramp to obtain the desired pore size and porosity (from 25 °C to -25 °C and from -25°C to 25 °C in 50 min, $p = 0.20$ mbar). The morphology of the scaffold was characterized by scanning electron microscopy (SEM) and the pore size determined by ImageJ (US National Institutes of Health); the swelling properties of the scaffold and overall porosity were determined through water and ethanol infiltration methods (Minardi et al., 2014). Mean diameters were determined by caliper measurement. All analyses was performed both on control scaffolds and on scaffolds after a 10 days culture with MCF-7 and MDA-MB-231 (after a decellularization step).

4.3 Cell seeding and culture

MCF-7 and MDA-MB-231 cell lines were obtained from the American Type Culture Collection (USA). All cells were maintained in DMEM medium supplemented with 10% fetal bovine serum, 1% penicillin-streptomycin and 1% glutamine (PAA, USA) at 37°C in a 5% CO₂ atmosphere. Each scaffold was placed in a 6-multiwell plate and seeded with 5×10^4 cells by dropping 50 µl of the cell suspension on the scaffold. Cells were allowed to adhere for 1 h at 37°C, after which 4 ml of culture medium were gently added to each well. After a 24-h incubation, all scaffolds were carefully removed and placed in a new 6-multiwell plate. Medium was replaced daily. Uncellularized control scaffolds were maintained in cell-free culture medium at the same temperature and humidity conditions.

4.4 Cell quantification

The number of cells that infiltrated the scaffold at day 10 was assessed by total DNA content quantification using the PicoGreen dsDNA assay (Invitrogen, Carlsbad, CA, USA). The total DNA was extracted using DNeasy Blood & Tissue Kit (Qiagen, Duesseldorf, Germany) following the manufacturer's instructions and 100 μ L of DNA mixture were then added to 100 μ L of PicoGreen reagent working solution. Fluorescence of the samples was measured with a microplate reader (FLUOstar OPTIMA BMG LABTECH, Ortenberg, Germany) with excitation and emission wavelengths of 480 and 520 nm, respectively. The total number of cells was determined using the conversion factor of 7.7 pg DNA/cell.

4.5 Histological analysis

The collagen constructs were fixed in 10% neutral buffered formaldehyde and dehydrated in a graded series of ethanol. Samples were then embedded in paraffin, sliced at a thickness of 5 μ m with a rotating microtome (Leica Biosystems, USA) and mounted on Superfrost Plus microslides (Thermo Fisher Scientific, USA). Hematoxylin and eosin (H&E) staining was performed to evaluate cell morphology and distribution in the scaffold matrix.

4.6 LOX inhibition

The activity of LOX was blocked by the irreversible LOX inhibitor, β -aminopropionitrile (BAPN) (Sigma Aldrich) (Nilsson et al., 2016; Yang et al., 2013 and Bondareva et al., 2009). MDA-MB-231 within the scaffold were treated with 500 μ M BAPN after 24 hours from the seeding. Administration of BAPN was performed daily until the end of the experiment. At day 10 the culture was stopped, cell proliferation in the presence or absence of LOX inhibition was assessed by MTT assay and the mechanical test was performed.

4.7 Scaffold decellularization

The scaffolds were decellularized in 0.5% Triton X-100 for 1 h at room temperature and then washed 3 times in phosphate saline buffer (PBS). Uncellularized scaffolds were exposed to the same decellularization process to ensure that the experimental conditions did not contribute to modify the scaffold's mechanical properties. Decellularization was confirmed by the absence of MTT metabolism. The remaining DNA content of the decellularized scaffolds was assessed as follows: total DNA was extracted using the DNeasy Blood & Tissue Kit (Qiagen, Germany) following the manufacturer's instructions and quantified with a NanoDrop ND-1000 spectrophotometer.

4.8 Development of the low-force testing device

We developed a prototype loading device to apply a state of unconfined uniaxial compression to the collagen scaffolds (**Figure 11**). This in-house built instrument consisted of a base support with a cylindrical hole (diameter 10 mm, depth 0.5 mm)

designed to lodge the scaffold specimen, and a cylindrical piston (diameter 10.1 mm) to indent the specimen with known force values. The applied stress (in kPa) could then be computed by dividing the applied force by the cross section of the specimen. The applied force consisted of a pre-load of 0.09 Newton (corresponding to a pre-stress of 1.8 kPa), which was held constant for 30 seconds; the full load of 0.38 Newton (corresponding to 7.6 kPa) was then constantly applied for 30 seconds. Such holding times were sufficient for the visco-elastic time-dependent deformation to reach an equilibrium. The piston was equipped with a dial gauge (Borletti, Milan, Italy) to measure the piston displacement while the specimen was compressed. The consequent strain (dimensionless) was computed by dividing the measured piston displacement by the height of the specimen. The dial gauge had a resolution of 0.002 mm (corresponding to a resolution of 0.1% for the strain).

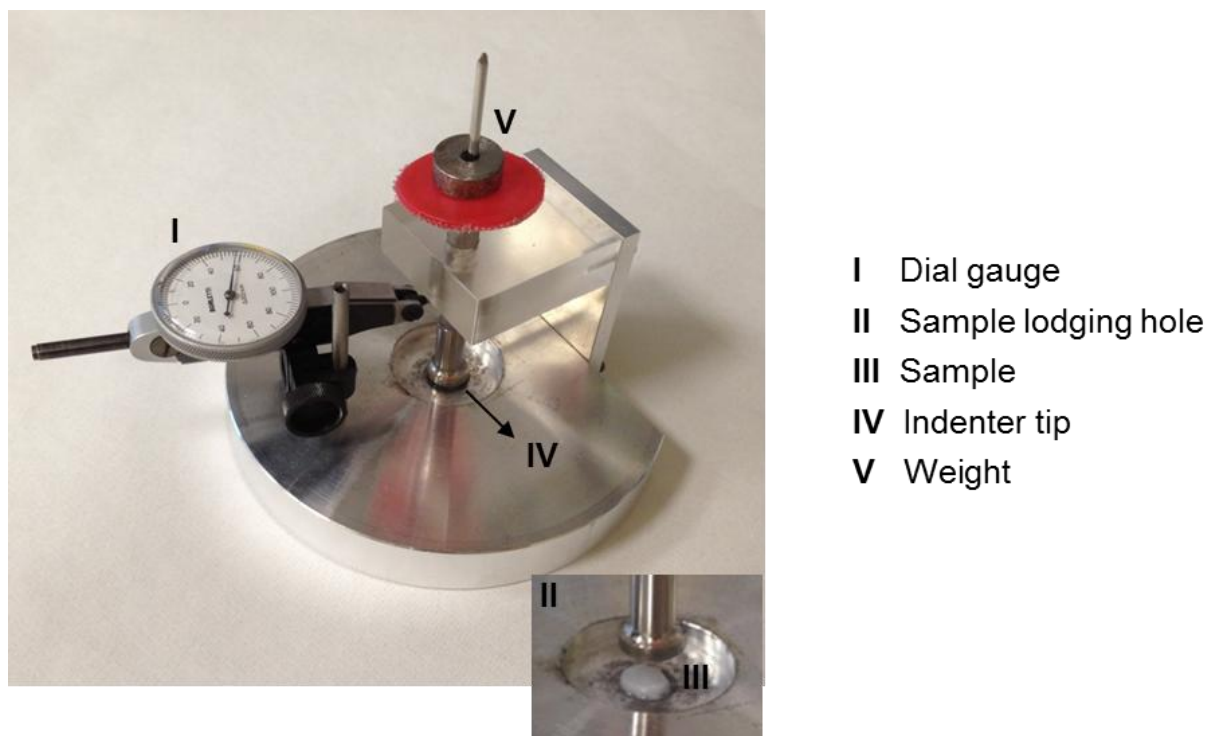


Figure 11. Photo of the low-force mechanical testing device developed to measure the compressive modulus of the collagen scaffolds.

4.9 Mechanical testing

4.9.1 Low-force testing device

Prior to any measurements the scaffolds were decellularized in 0.5% Triton X-100 for 1 h at room temperature and then washed 3 times in phosphate saline buffer (PBS). Uncellularized scaffolds were exposed to the same decellularization process to ensure that the experimental conditions did not contribute to modify the scaffold's mechanical properties. The specimens were tested in air immediately after having been removed from the PBS where they were soaked. For each sample, the pre-load of 0.09 Newton was constantly applied for 30 seconds, followed by the full load of 0.38 Newton, applied for other 30 seconds. The stiffness (compressive modulus, in kPa) of the collagen scaffold was computed as the ratio between the increment of stress and increment of strain from the pre-load to the full load values (Beer et al., 2011). The compressive modulus of collagen scaffolds decellularized after a 10-day culture with MCF-7 or MDA-MB-231 was compared with that of uncellularized scaffolds. Five specimens of each type were tested. Each specimen was tested 10 times to improve the quality of the measurement. The compressive modulus of each specimen was computed as the average of the 10 repeated measurements.

4.9.2 Dynamic Mechanical Analysis (DMA)

Compression tests were carried out also by dynamic mechanical analysis (DMA) using a Q800 instrument (Norleq, Portugal) (**Figure 12**), a standard methodology to characterize the mechanical properties of the scaffolds. As described before, prior to any measurements the scaffolds were decellularized in 0.5% Triton X-100 for 1 h at room temperature and then washed 3 times in phosphate saline buffer (PBS). Uncellularized scaffolds were exposed to the same decellularization process to ensure that the experimental conditions

did not contribute to modify the scaffold's mechanical properties. Sample length and diameter were measured with a caliper before each testing. The measurements were performed under compression mode, following cycles of constantly increasing loads, ranging from 0 to 0.01N. The test were carried out at room temperature. For each sample measurements were performed in 5 technical replicates for two biologically independent experiment.



Figure 12. Photo of the Dynamic Mechanical Analysis instrument used to measure the compressive modulus of the collagen scaffolds.

4.9.3 Atomic Force Microscopy (AFM) analysis

The MultiModeNanoscope 8 (Bruker) atomic force microscope was used to perform the nanoindentation test (**Figure 13**). This instrument is an ultra-high resolution material

science microscope, equipped with ScanAsyst and PeakForce Quantitative Nanomechanical imaging modes and Peak Force Tapping technology. This microscope allowed for the determination of the mechanical characteristic of single collagen fibers. Fibers were removed from the bulky scaffold, suspended in MQ water and let dry on a mica surface. A sharp, rigid tip was used for probing the fiber mechanical properties. AFM images were collected using single-beam silicon cantilever probes (nominal tip radius of curvature 10 nm, force constant 0.65 N/m, tip half angle 18°C) from different samples and at random spot surface sampling (at least five areas per each sample). Quantitative mechanical characterization was determined under peak-force tapping mode with 1.0 Hz scan rates and a 200 mV amplitude set point. The DMT model (Derjaguin et al., 1975) was applied to calculate the Young's modulus. Several fibers were indented for each scaffold to calculate their strength.



Figure 13. The Atomic Force Microscope used to measure the mechanical properties of single collagen fibers.

4.10 Microscopy analysis

The collagen scaffolds were imaged by SEM and Laser Confocal Microscopy. For SEM imaging, samples were washed in 0.1 M sodium cacodylate buffer pH 7.4 and fixed in 2.5% glutaraldehyde in 0.1 M sodium cacodylate buffer pH 7.4 for 2 h at 4°C. Samples were then dehydrated in a graded series of ethanol, desiccated and sputter-coated with platinum. Images were acquired with a Nova NanoSEM (FEI, USA). For confocal imaging, cells were washed in 1% PBS, fixed with 4% paraformaldehyde for 20 min at room temperature and stained with 10 μ M/ml DRAQ5™ (ImmunoChemistry Technology, Bloomington, MN, USA). Images were acquired with an A1 laser confocal microscope (Nikon Corporation, Tokyo, Japan), and analyzed with the NIS Elements software (Nikon Corporation, Tokyo, Japan).

4.11 Quantitative Real-Time Reverse Transcription-PCR (qRT-PCR)

Total mRNA was isolated using TRIzol Reagent (Invitrogen, USA) following the manufacturer's instructions. Five hundred nanograms of RNA were reverse-transcribed using the iScript cDNA Synthesis Kit (BioRad, USA). The final mixture was incubated at 25°C for 5 min, 42°C for 20 min, 47°C for 20 min, 50°C for 15 min and finally a 85°C for 5 min. Real Time-PCR was performed in a 7500 Real-Time PCR System (Applied Biosystems, USA) using the TaqMan universal assay mix (Applied Biosystems). Amplification was performed in a final volume of 20 μ l containing 2x Gene Expression Master Mix (Applied Biosystems) and 2 μ l of cDNA. The reaction mixtures were all subjected to 2 min at 50°C, 10 min at 95°C followed by 40 PCR cycles at 95°C for 15 s and 60°C for 1 min. The stably expressed endogenous β -actin and HPRT were used as reference genes. Three target markers were analyzed: vimentin (VIM), E-cadherin

(CDH1) and lysyl oxidase (LOX). The amount of these transcripts was normalized to the endogenous reference genes and expressed as n-fold mRNA levels relative to a calibrator using the comparative threshold cycle (Ct) value method ($\Delta\Delta Ct$). For all analysis the calibrator used was a mix of the RNA extracted from MCF7 and MDA-MB-231 in standard monolayer culture.

4.12 MTT assay

Cell survival in MDA-MB-231 treated with the LOX inhibitor BAPN was assessed by MTT assay. Briefly, the scaffolds were incubated for 2 hours at 37°C in 0.5 mg/ml of MTT solution (Sigma Aldrich). After solubilization in acidic isopropanol, the absorbance was read at 550 nm. The cell survival was determined comparing the average absorbance of cells in the absence or presence of BAPN treatment.

4.13 Drug testing

Doxorubicin (DOXO) was administered in monolayer cultures or in the 3D scaffolds at the following concentrations: 0.8, 1.6 and 4 $\mu\text{g/ml}$. Cells were cultured for 24 h before exposure to the drug. Cell viability was assessed by MTT assay, as previously described. Survival percentages were calculated as the average absorbance of cells at each DOXO dose over the absorbance of untreated cells.

4.14 Xenograft study

To establish orthotopic breast tumors, MCF-7-Luc2 and MDA-MB-231-Luc2 cells, both marked with a luciferase probe, were suspended in 100 μ l of matrigel (BD, USA) at a concentration of 5×10^{12} cells and orthotopically injected into the right mammary fat pad of 8 week-old female immunodeficient nu/nu nude mice (n. 5 animals for each cell line). Tumor growth was followed by *in vivo* bioluminescence imaging and caliper measurement every 2-3 days after the injection. After 4 weeks, tumors were resected and embedded in Optimal Cutting Temperature (OCT) compound and cryo-sectioned. All experimental animal procedures were reviewed and approved by the Institutional Animal Care and Use Committee (IACUC) of the Houston Methodist Research Institute (HMRI) protocol number AUP 0614-0033.

4.15 Collagen staining

Trichrome staining and picrosirius red were performed on the OCT embedded frozen tissues to study the tumor collagen matrix and on the collagen scaffold sections. Trichrome staining (Abcam) was performed according to manufacturer's instructions. For picrosirius red the frozen sections were stained with 0.1% (Direct Red 80) (Sigma Aldrich) sirius red in saturated aqueous solution of picric acid and counterstained with Weigert's hematoxilin. The RGB images were analyzed by ImageJ. At least n. 5 images per group were analyzed to quantify the collagen content.

4.16 Statistical analysis

At least three independent experiments were performed. Data are presented as mean \pm standard error (SE), with n indicating the number of replicates. For *in vitro* and *in vivo* data, differences between groups were assessed by a two-tailed Student's t-test and accepted as significant at $p < 0.05$.

5. Results

5.1 Collagen remodeling in breast xenograft tumors

Orthotopic implantation of MCF-7 and MDA-MB-231 in female immunodeficient mice was performed to investigate the collagen content and architecture in the ECM of *in vivo* breast tumors. After 4 weeks both cell lines had developed detectable mammary tumors. Bioluminescence imaging and caliper measurement showed that MCF-7 grew considerably slower than MDA-MB-231 displaying a mean tumor volume of $70 \pm 15 \mu\text{m}^3$ compared to $388 \pm 68 \mu\text{m}^3$ for MDA-MB-231 (Figure 14a and 14b).

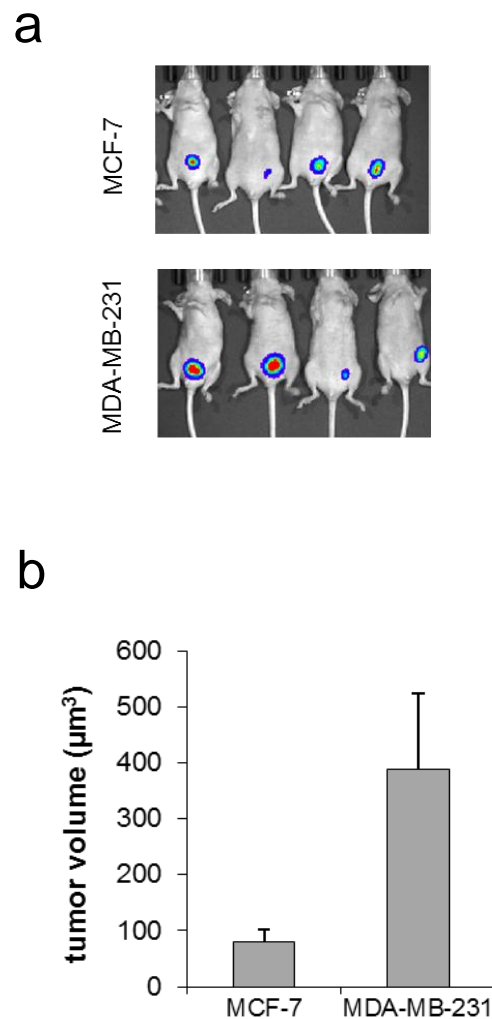


Figure 14. Bioluminescence imaging (a) of mammary tumors in nude mice (n=5 for each group) generated by orthotopic injection of MCF-7 or MDA-MB-231 and caliper measurement (b) of tumor volume after 4 weeks (μm^3).

Trichrome staining of resected tumor sections revealed a higher presence of thick collagen fibers in MDA-MB-231 orthotopic tumors compared to those generated by MCF-7 (**Figure 15a**). Moreover, quantification of the collagen percentage in picrosirius red-stained sections showed that MDA-MB-231 tumors displayed a significantly higher collagen content than that of MCF-7 ones ($p = 0.0005$) (**Figure 15b**). Finally, the *in vivo* expression of the matrix crosslinking enzyme LOX was markedly higher for MDA-MB-231 than for MCF-7 (**Figure 15c**).

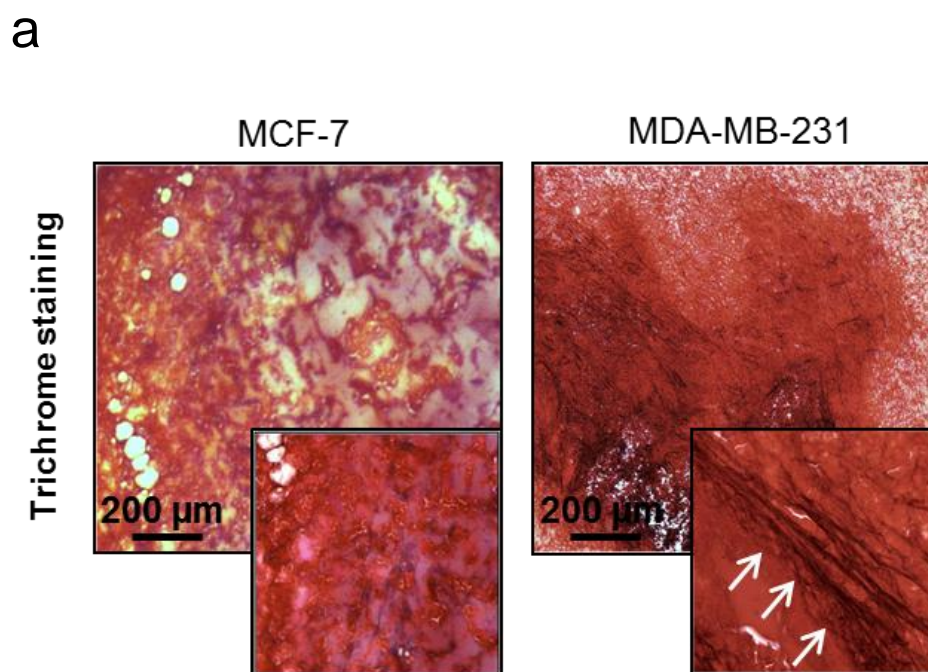


Figure 15. (a) Trichrome staining of OCT-embedded xenograft breast tumors generated from orthotopic injection of MCF-7 and MDA-MB-231.

b

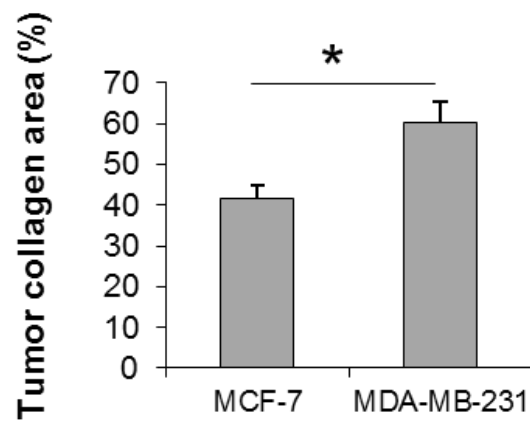
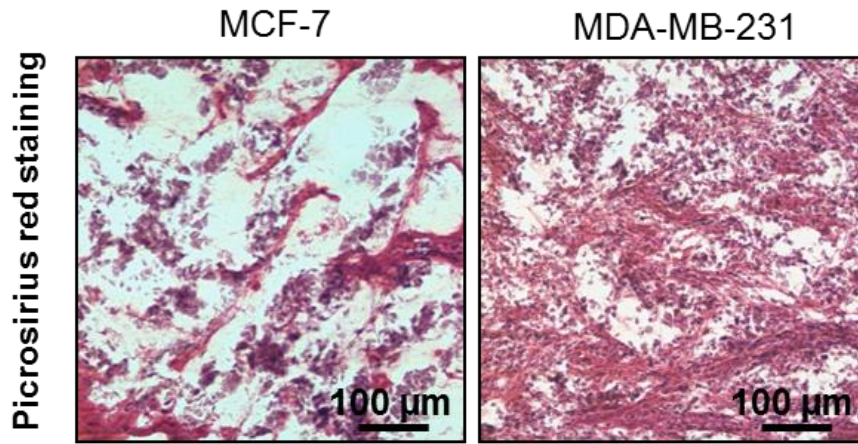


Figure 15. (b) Picrosirius red staining of OCT-embedded xenograft breast tumors generated from orthotopic injection of MCF-7 and MDA-MB-231, and quantification of the mean percentage of collagen to total area.

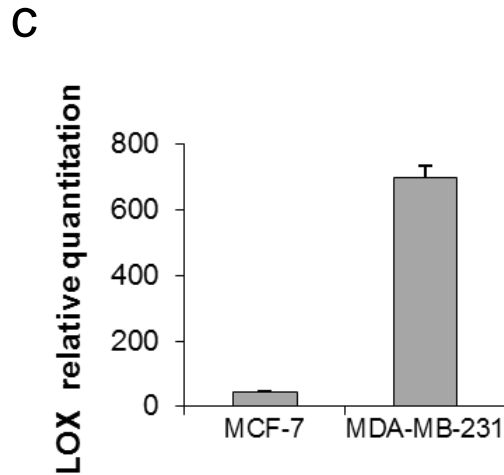


Figure 15. (c) relative quantitation values of LOX in MCF-7 and MDA-MB-231 orthotopic tumors. Data are mean \pm SE. * $p < 0.05$.

5.2 Collagen scaffold macro- and micro- structural properties

Type I collagen scaffolds showed a mean diameter of 9 ± 0.5 mm (**Figure 16a**) and were 2 mm thick. The pH-driven method, through which the collagen scaffolds were synthesized, enabled the production of a biomimetic material with highly reproducible morphology and tunable macro- and micro-structure, as characterized by Scanning Electron Microscopy (SEM). The size of the pores ranged between 150 to 300 μm , with a mean pore size of 197 ± 25 μm (**Figures 16b and 16c**). Collagen fibers showed a high degree of structural assembling and preserved their typical D-bands (arrowhead), (**Figure 16d**) a characteristic axial D-periodic (67 nm) morphology derived from the self-assembly of single collagen molecules. The scaffolds displayed a mean porosity percentage of 87.8 ± 4.1 (**Table 1**). The average pore volume was $25 \times 10^3 (\pm 1300)$ μm^3 , the average pore diameter was 197 (± 25) μm and the pore walls were 15 (± 1.0) μm thick (**Table 1**).

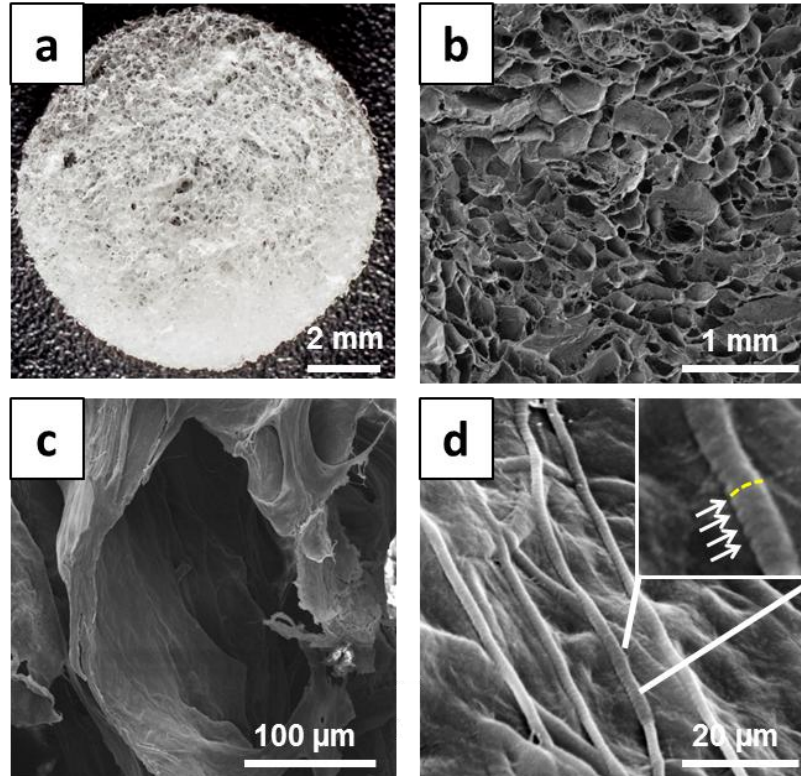


Figure 16. (a) Pictures of the collagen-based scaffold; (b-d) SEM analysis of the scaffolds at different magnifications with the typical D-bands (d) identified by white arrows and a yellow dotted line to show their axial disposition.

Table 1.

Physical properties of the collagen scaffolds.

	Average	SD
Scaffold Volume (μm^3)	$57.7 \cdot 10^3$	± 4.5
Pore area (μm^2)	$24.7 \cdot 10^3$	± 1.3
Volume of collagen (μm^3)	$8.8 \cdot 10^3$	± 0.5
Void space (μm^3)	$48.9 \cdot 10^3$	± 0.2
Porosity (%)	87.8	± 4.1
Average porosity diameter (μm)	197	25
Pore wall thickness (μm)	14.7	± 1.0

5.3 Phenotypes and behavior of breast cancer cells on the collagen matrix

The porous structure of the collagen matrix allowed for cell penetration throughout the scaffold, as detected by the MTT assay at 10 days of culture. The MTT assay is a colorimetric assay for measuring cell metabolic activity, reflecting the number of present viable cells. Cellular oxidoreductase enzymes are capable of reducing the tetrazolium dye MTT 3-(4,5-dimethylthiazol-2-yl)-2,5-diphenyltetrazolium bromide to insoluble formazan, which has a purple color. After 10 days of culture with MCF-7 or MDA-MB-231, the scaffold, stained with the tetrazolium dye MTT, appeared homogeneously purple-colored, indicating that cancer cells had penetrated throughout the material and populated all the scaffold regions. Conversely, the MTT dye was not reduced in empty control scaffolds (Figure 17).

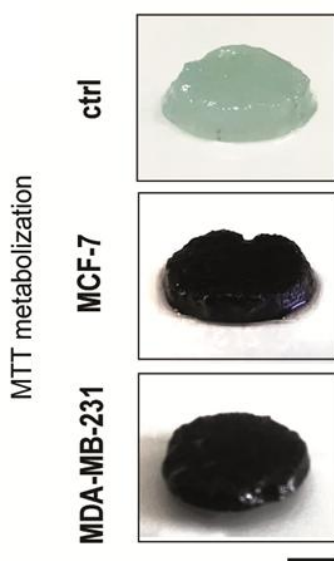


Figure 17. MTT assay of MCF-7 and MDA-MB-23 cultured on the 3D scaffold, compared to an empty control scaffold (ctrl). Scale bars: 3 mm.

While MCF-7 are associated with weak invasiveness, MDA-MB-231 are enriched for epithelial to mesenchymal transition (EMT) markers and display a more invasive behavior. When cultured on collagen scaffolds, the two cell lines generated tissue-like

structures and maintained their distinctive features: MCF-7 displayed an epithelial-like morphology with a tightly cohesive cobblestone appearance, while MDA-MB-231 showed a mesenchymal phenotype with lower cell-to-cell contact and a spindle appearance (**Figure 18a**). Both cell lines proliferated within the scaffold, and at day 10 the number of cells reached about 9×10^6 for MCF-7 and 9.8×10^6 for MDA-MB-231 (**Figure 18b**). Gene expression analysis showed that MCF-7 had a high level of E-cadherin expression but low vimentin, while MDA-MB-231 showed lower levels of E-cadherin and a high vimentin expression (**Figure 18c**).

a

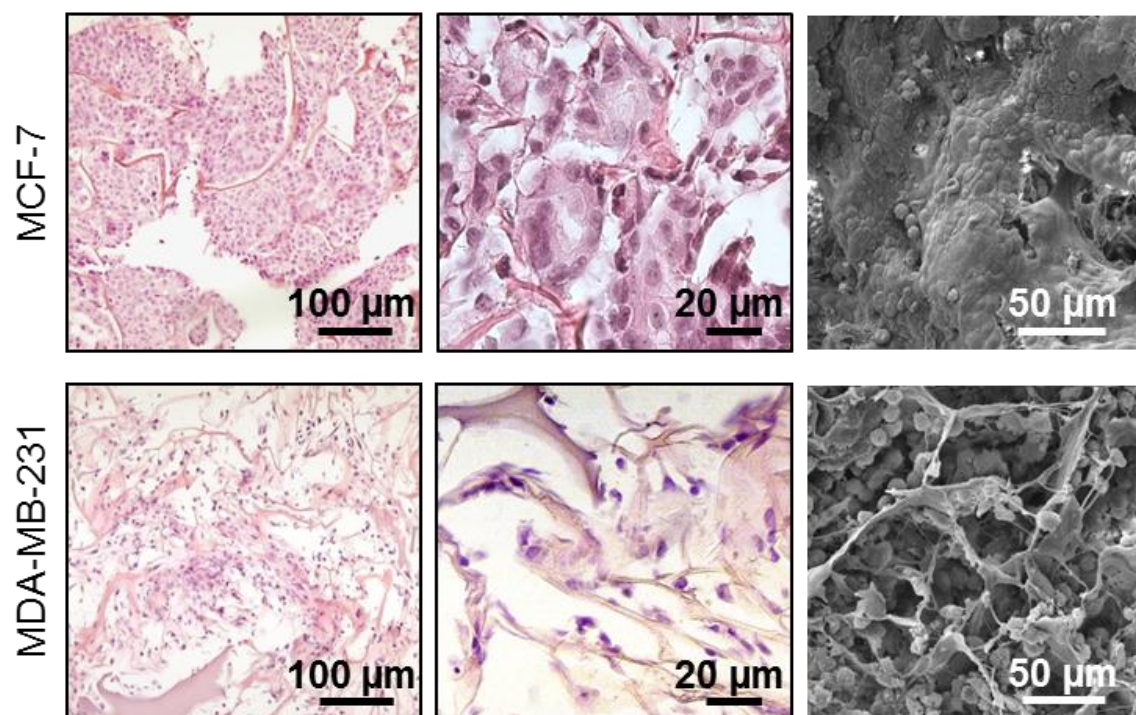


Figure 18. (a) Hematoxylin & eosin staining of paraffin-embedded sections of the 3D scaffolds cultured with MCF-7 or MDA-MB-231, and SEM imaging of scaffolds cultured with MCF-7 or MDA-MB-231.

b

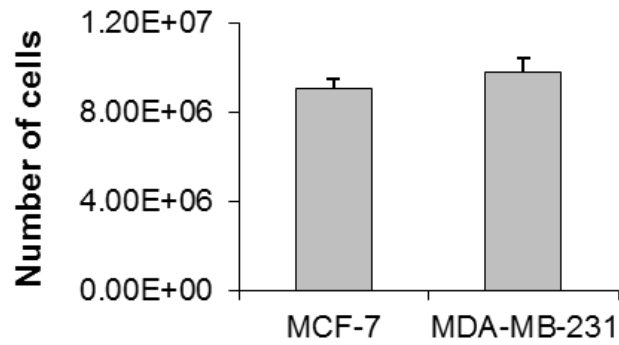


Figure 18. (b) number of MCF-7 and MDA-MB-231 that infiltrated the collagen scaffold at day 10 of culture.

c

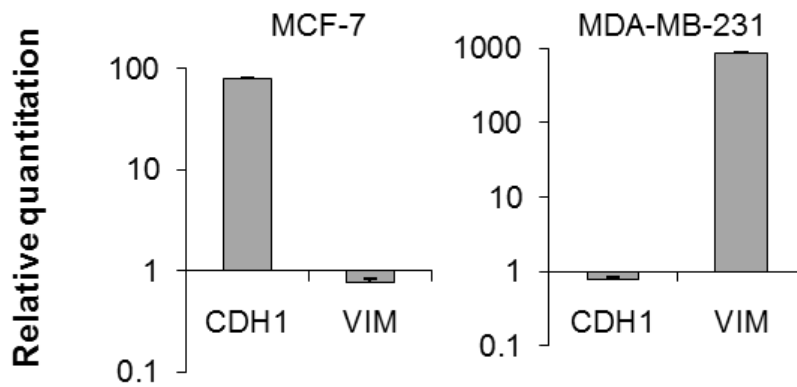


Figure 18. (c) Relative quantitation values of E-cadherin (CDH1) and vimentin (VIM) in MCF-7 and MDA-MB-231 cells.

Confocal microscopy analysis of cellularized scaffolds showed MCF-7 aggregated in clusters with epithelial-like morphology and higher cell-cell contact (**Figure 19a**). Conversely, MDA-MB-231 cells displayed a spindle shaped mesenchymal phenotypes, limited cell to cell contact and an aligned distribution (arrowhead) over the collagen fibrils, resembling a clinical feature of invasive lobular breast tumors known as “Indian filing” (Provenzano et al., 2006) (**Figure 19b**). DAPI-stained frozen sections of the 3D scaffold revealed that in MCF-7 the cell distribution over core and rim areas remained similar between day 1 and day 7 (**Figure 19c**). Conversely, this distribution was significantly different ($P = 0.023$ and $P = 0.046$ at day 1 and 7, respectively) for MDA-MB-231 cells that radially concentrated at the rim of the scaffold over time (**Figure 19d**). This result, together with the Indian file distribution, suggested the activation of a collective migratory process toward the scaffold’s edges.

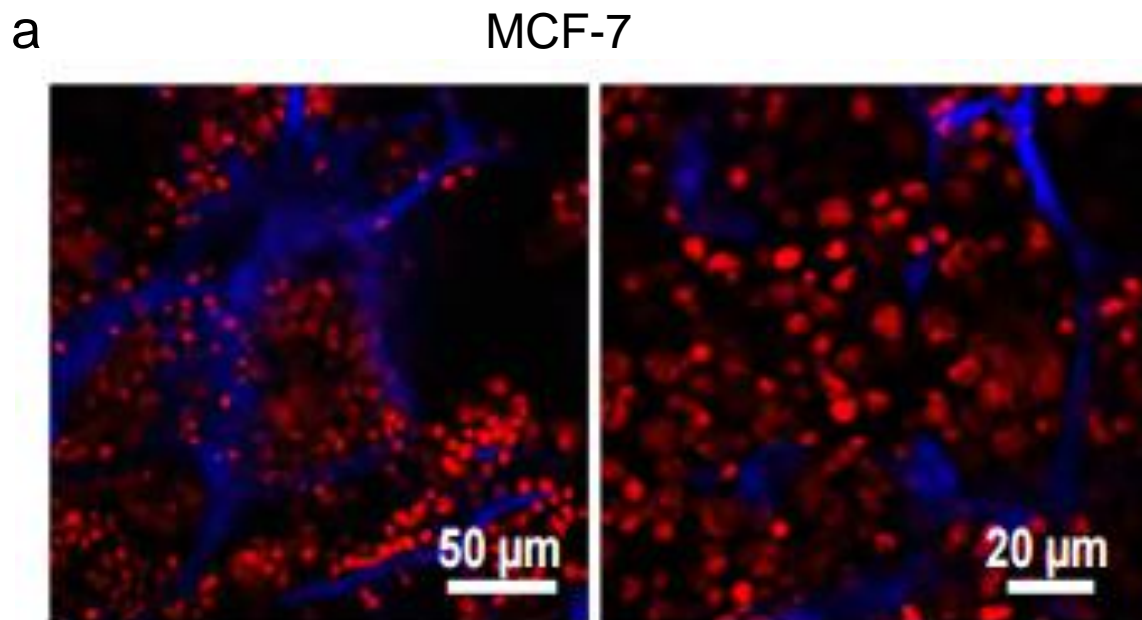


Figure 19. (a) Confocal microscopy images at different magnifications of MCF-7 within the scaffold (3D) at day 7. Cells are stained with DRAQ5 (red) and blue is the collagen scaffold autofluorescence.

b

MDA-MB-231

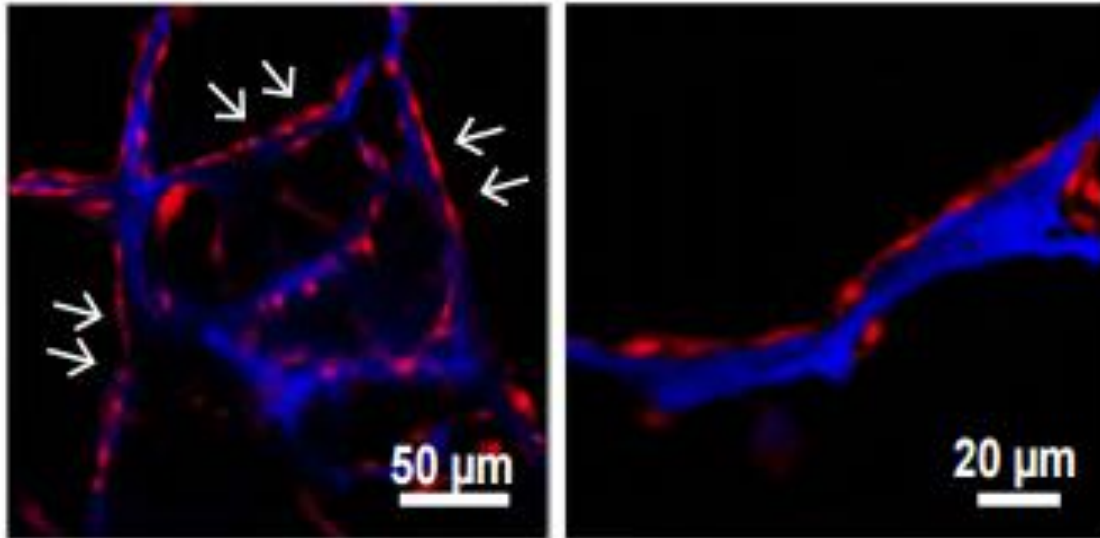


Figure 19. (b) Confocal microscopy images at different magnifications of MDA-MB-231 within the scaffold (3D) at day 7. Cells are stained with DRAQ5 (red) and blue is the collagen scaffold autofluorescence.

c

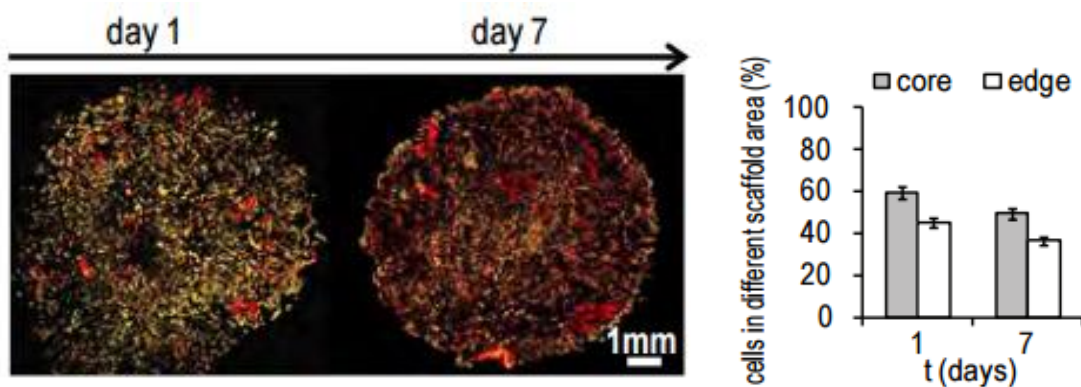


Figure 19. (c) Whole images of histological sections of 3D cultured MCF-7 at day 1 and 7, and percentages of cells in edge or core regions of the scaffold. Cells are stained with DAPI (yellow) and red is the collagen scaffold autofluorescence. Data represent mean \pm S.D. (n = 3) *p < 0.05, two-tailed Student's t-test.

d

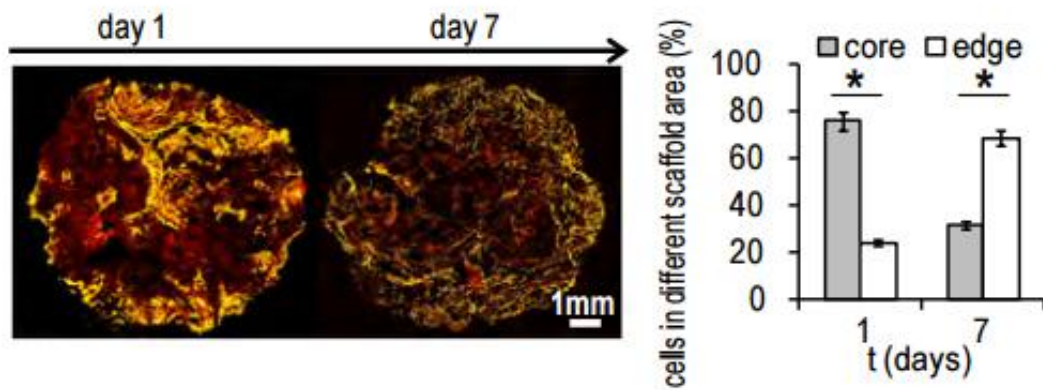


Figure 19. (d) Whole images of histological sections of 3D cultured MDA-MB-231 at day 1 and 7, and percentages of cells in edge or core regions of the scaffold. Cells are stained with DAPI (yellow) and red is the collagen scaffold autofluorescence. Data represent mean \pm S.D. (n = 3) *p < 0.05, two-tailed Student's t-test.

MDA-MB-231 proved capable of internalizing collagen: confocal images of the scaffold matrix showed the presence of blue collagen spots in the scaffolds cellularized with MDA-MB-231. These signals were not detectable in empty scaffolds or in the presence of MCF-7 cells (**Figure 20a**). The collagen spots demonstrated an intracellular localization that was further highlighted in images processed with ImageJ software (**Figure 20b**).

a

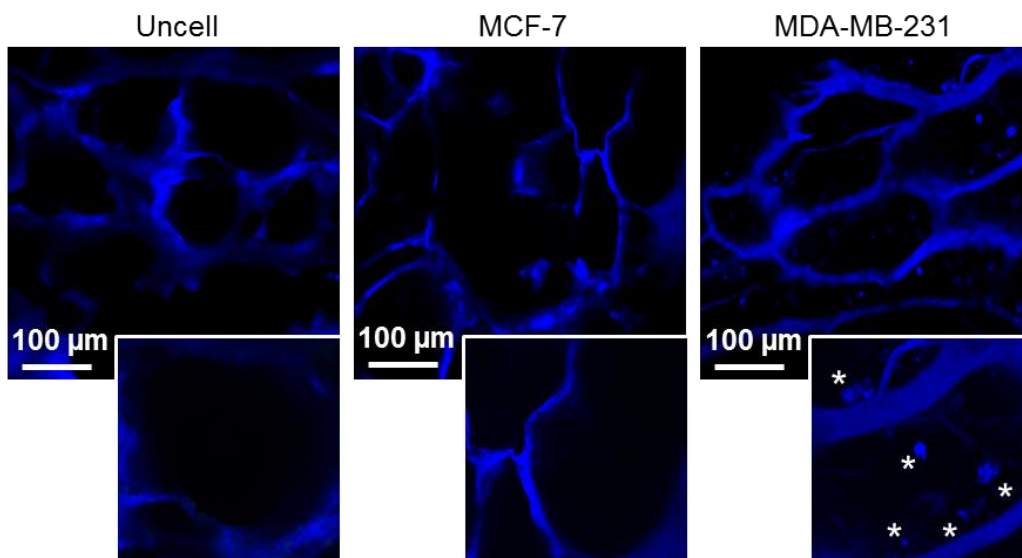


Figure 20. (a) Confocal images of the collagen matrix (blue, autofluorescence) of an empty scaffold (uncell), and of scaffolds cellularized with MCF-7 or with MDA-MB-231

b

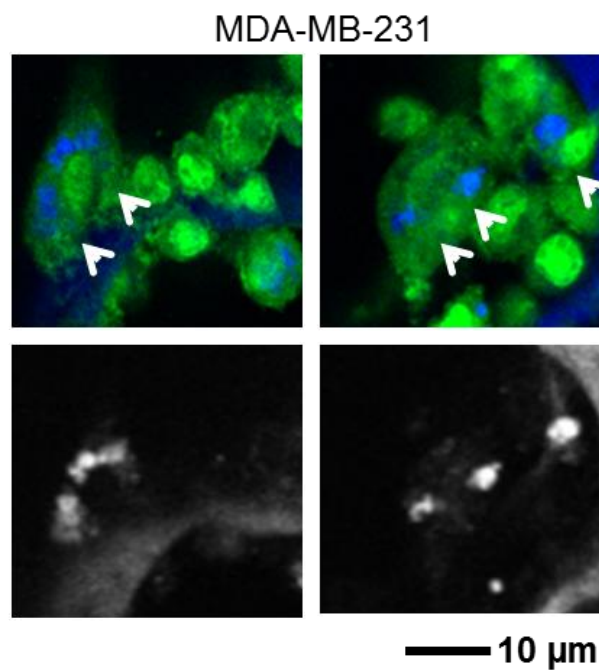


Figure 20. (b) Confocal microscopy analysis of GFP-labeled MDA-MB-231 (green, GFP) on collagen scaffolds (blue, autofluorescence) and processed images to exclude the cell signal.

Finally, culturing within the scaffold model affected the sensitiveness of cancer cells to Doxorubicin (DOXO): both cell lines showed a decreased sensitivity to DOXO compared to that of monolayer cultures, as proven by the higher survival rates observed in all tested concentrations (**Figure 21**). MCF-7 within the 3D model proved to be completely resistant to DOXO at the highest tested concentration (4 $\mu\text{g/ml}$).

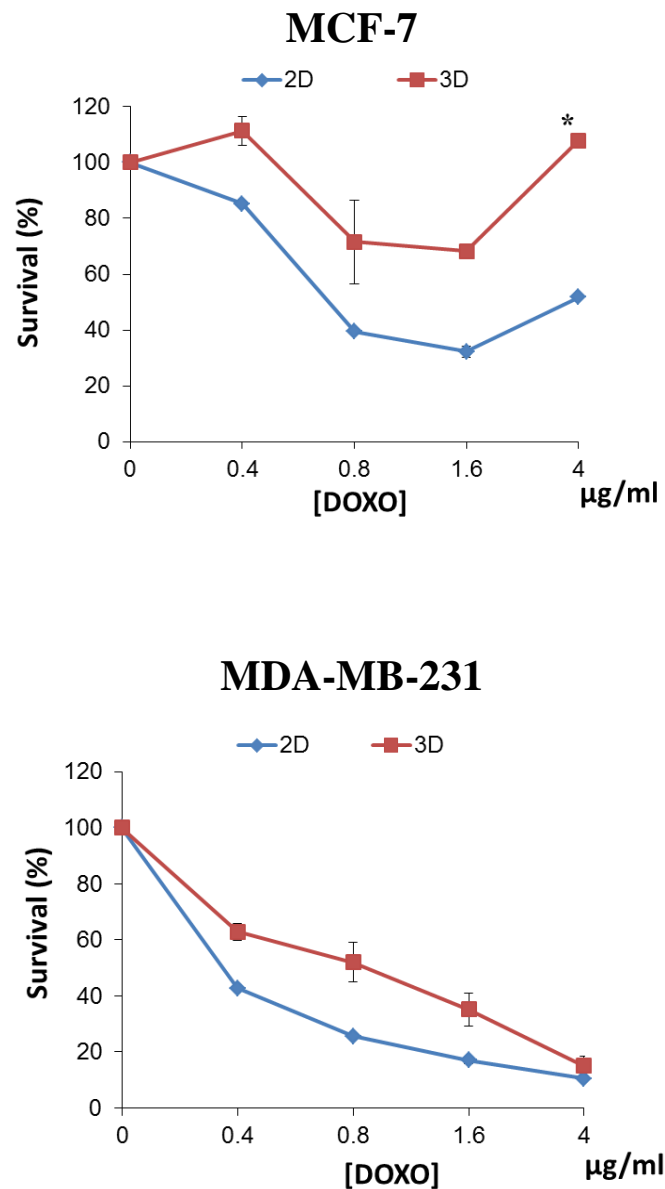


Figure 21. Percentages of survival of MCF-7 and MDA-MB-231 after 3 days of DOXO treatment at different concentrations in monolayer culture (2D) or within the scaffold (3D).

5.4 Assessment of the low-force testing device repeatability

Preliminary tests were performed on scaffolds cultured with MDA-MB-231 to evaluate the repeatability of the measures obtained with the prototype loading device. The instrument and setting conditions exhibited good consistency that resulted in homogeneous dispersion of the different measures, as well as of the average values of technical replicates (**Figure 22**). The intra-assay coefficient of variation was 10.7 %, which was deemed sufficient for our purposes. No conditioning effect was detected when the same specimen was repeatedly loaded, as it can be observed in **Table 2a and b**.

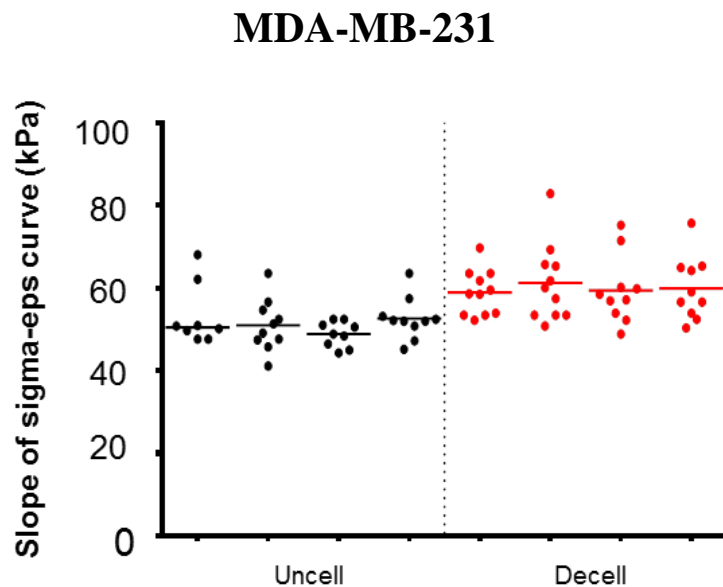


Figure 22. Stiffness values for uncellularized (uncell) scaffolds or for scaffolds decellularized (decell) after a 10-day culture with MDA-MB-231, expressed as the slope of the sigma-epsilon curve (sigma-eps) (kPa).

Table 2a

Stress (kPa)	Strain (adimens)										mean	SE
4.56	0.111	0.125	0.139	0.109	0.101	0.121	0.117	0.105	0.120	0.111	0.116	0.013

Table 2b

Stress (kPa)	Strain (adimens)										mean	SE
4.56	0.098	0.096	0.107	0.090	0.098	0.093	0.090	0.082	0.110	0.106	0.098	0.009

The raw data of stress-strain of an empty scaffold (Table 2a) and a scaffold with MDA-MB-231 (Table 2b) (for each scaffold ten repeated measurements have been performed). As it can be noted, no pre-conditioning effect was observed and the data showed good reproducibility.

5.5 Alteration of the compressive stiffness of collagen scaffolds by invasive breast cancer cells

We investigated the effect of MCF-7 and MDA-MB-231 on the stiffness properties of collagen scaffolds by comparing the compressive modulus of uncellularized samples with that of samples decellularized after 10 days of culture with either cell line. The efficacy of the decellularization process was confirmed by MTT metabolization, which resulted almost absent in decellularized samples (Figure 23a). Furthermore, the residual DNA content in decellularized scaffolds resulted of 11.1 ± 4.9 ng/ μ l compared to 175.9 ± 16.46 ng/ μ l of cellularized ones (Figure 23b).

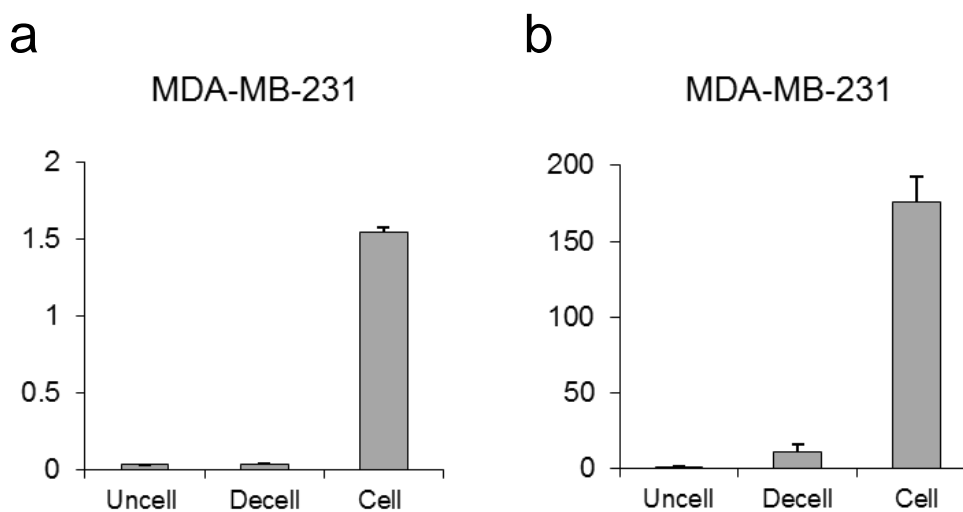


Figure 23. (a) 550 nm absorbance of uncellularized, cellularized (cell) or decellularized MTT-stained scaffolds; (b) DNA content (ng/μl) of uncellularized, cellularized or decellularized scaffolds.

MCF-7 did not significantly affect the mechanical properties of the scaffolds: uncellularized samples displayed an average compressive modulus of 47.1 ± 1.8 kPa, while samples decellularized after MCF-7 culture showed an average compressive modulus of 48.9 ± 1.3 kPa. Conversely, MDA-MB-231 cells produced a significant ($p=0.038$) increase in the scaffold stiffness: uncellularized samples displayed an average compressive modulus of 46.9 ± 2.7 kPa, while samples decellularized after MDA-MB-231 culture had an average compressive modulus of 57.9 ± 3.6 kPa (**Figure 24a**). Scaffold compressive modulus increased by 23% after MDA-MB-231 cell culture, in sharp contrast to the increase observed after culture with MCF-7 which was lower than 5% (**Figure 24b**). Finally, MDA-MB-231 within the collagen scaffolds showed around a 1000-fold higher expression level of LOX than MCF-7 (**Figure 24c**).

a

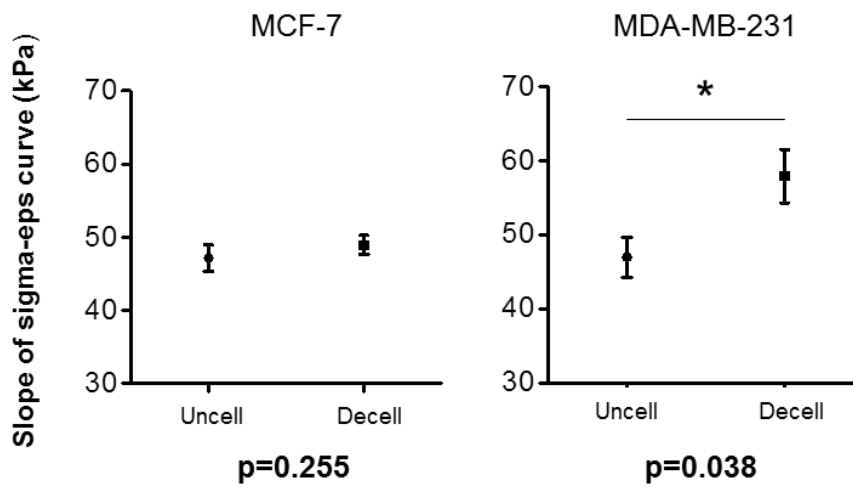


Figure 24. (a) Average slope of the sigma-eps curve (kPa) for uncellularized scaffolds or for scaffolds decellularized after a 10-day culture with MCF-7 or with MDA-MB-231. Data are mean \pm SE. * $p < 0.05$.

b

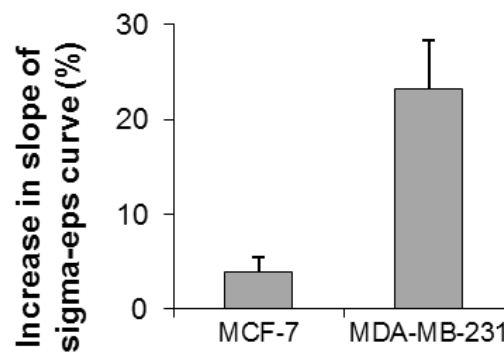


Figure 24. (b) Percentage increase in the slope of the sigma-eps curve for scaffolds decellularized after a 10-day culture with MCF-7 or MDA-MB-231 with respect to uncellularized scaffolds. Data are mean \pm SE.

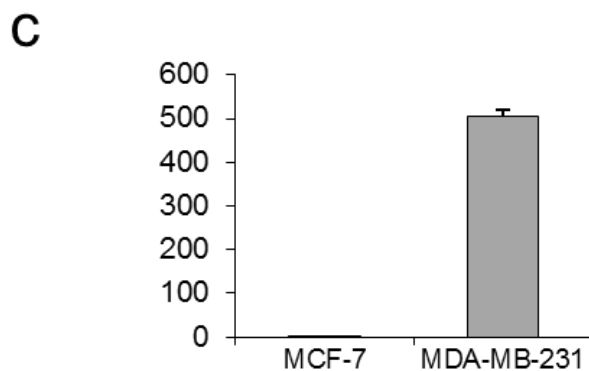


Figure 24. (c) Relative quantitation values of LOX in MCF-7 and MDA-MB231. Data are mean \pm SE. * $p < 0.05$.

5.6 Dynamic Mechanical Analysis of collagen scaffolds

Mechanical testing in compression was performed also by DMA, comparing uncellularized control scaffolds with scaffolds decellularized after 10 days of culture with MDA-MB-231. Under compression all scaffolds exhibited the typical behavior of elastomers. Three characteristic deformation stages were identified: a linear elastic stage, followed by a stress plateau and, finally, a densification stage, characterized by a strong increase in the slope of the stress-strain curves. Representative compression stress-strain curves of controls scaffold and scaffolds cultured with MDA-MB-231 are reported in **Figure 25a and b**.

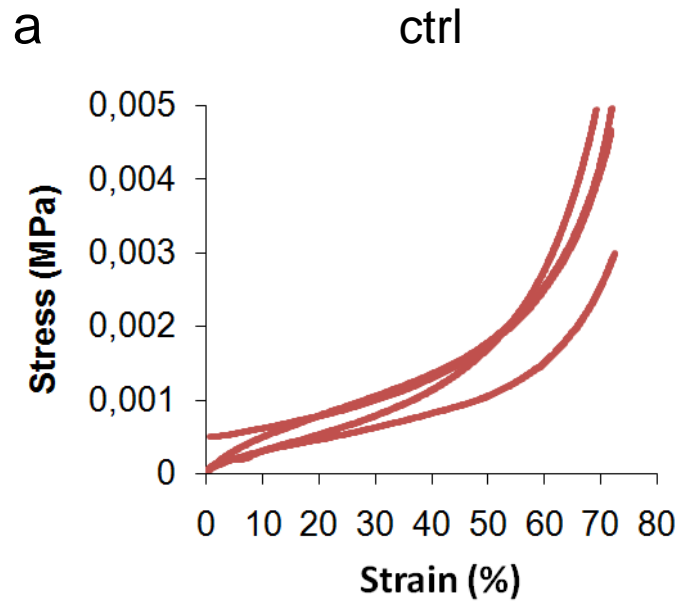


Figure 25. (a) Unidirectional compression stress (MPa) strain (%) curves of uncellularized collagen scaffolds.

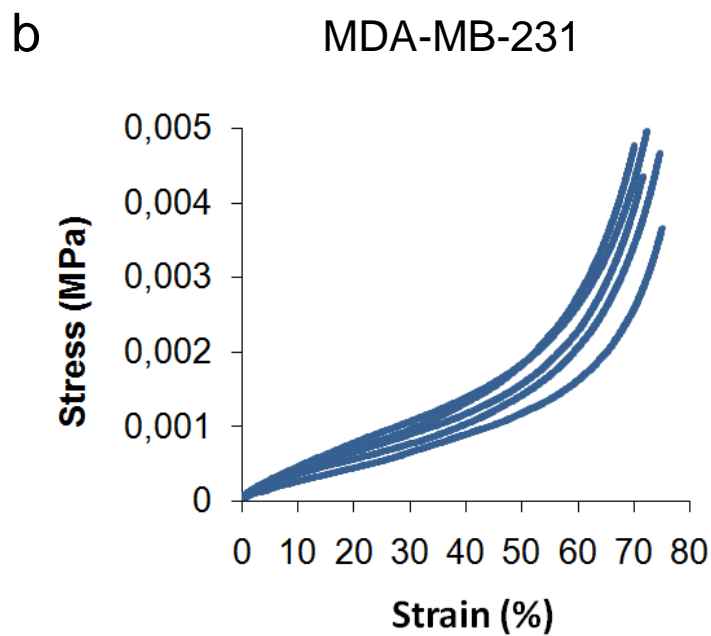


Figure 25. (b) Unidirectional compression stress (MPa) strain (%) curves of collagen scaffolds after a 10-day culture with MDA-MB-231.

The slope of the initial linear stage on the stress strain curves represents the compressive modulus of the scaffolds (**Figure 26a and b**).

a

ctrl

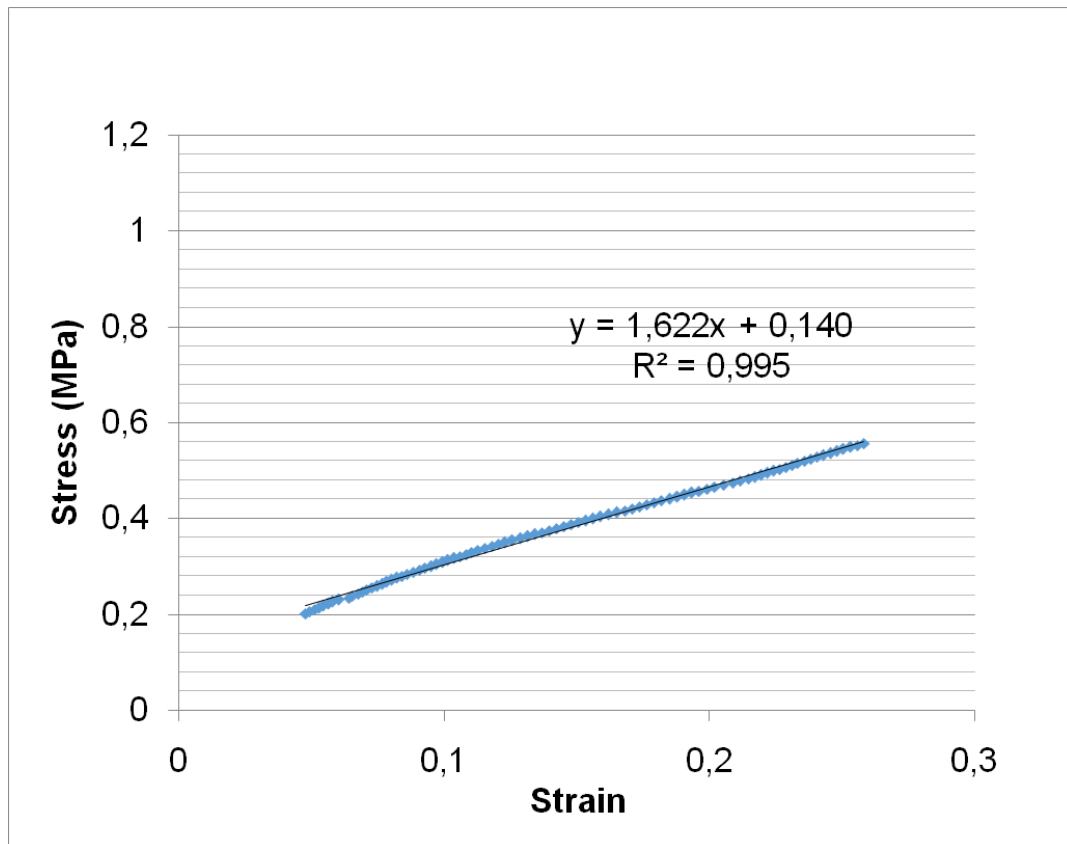


Figure 26. (a) Example of the initial linear stage of a compression stress (MPa) strain curve of uncellularized collagen scaffolds.

b

MDA-MB-231

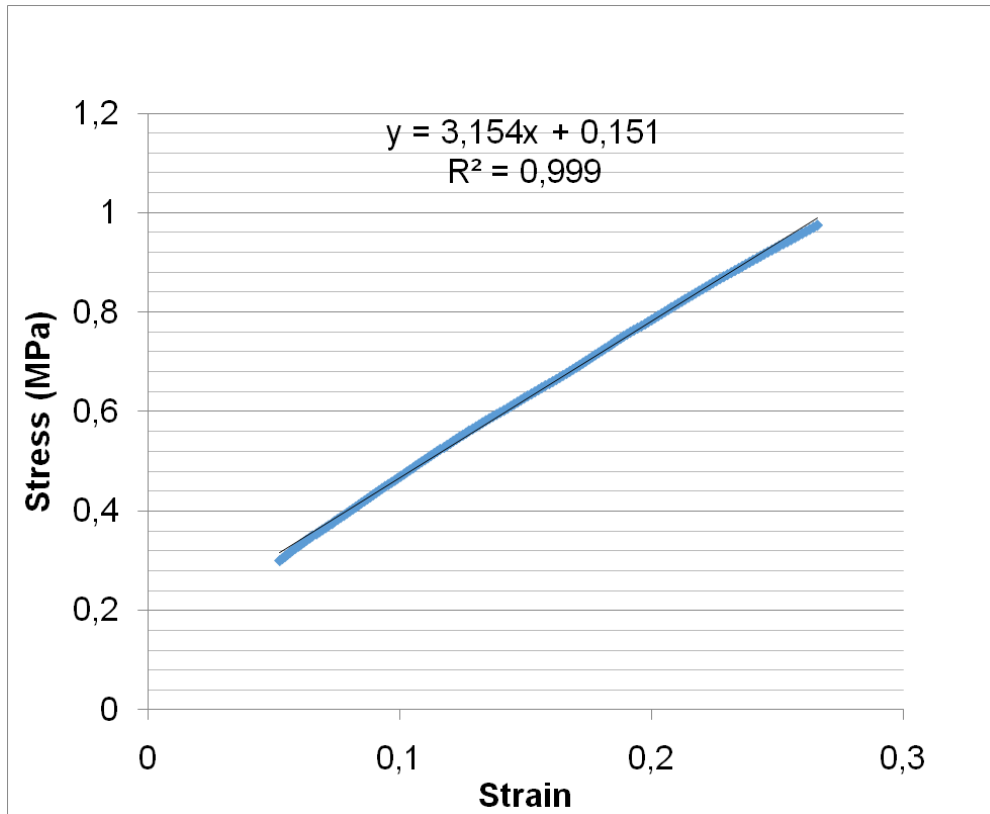


Figure 26. (b) Example of the initial linear stage of a compression stress (MPa) strain curve of collagen scaffolds after a 10-day culture with MDA-MB-231.

A 41% increase in the scaffold compressive modulus was observed after MDA-MB-231 culture: control samples displayed an average modulus of 1.7 ± 0.7 kPa, vs. 2.4 ± 0.4 kPa in samples cultured with MDA-MB-231 (**Figure 27**). This difference is not statistically significant ($p= 0.052$).

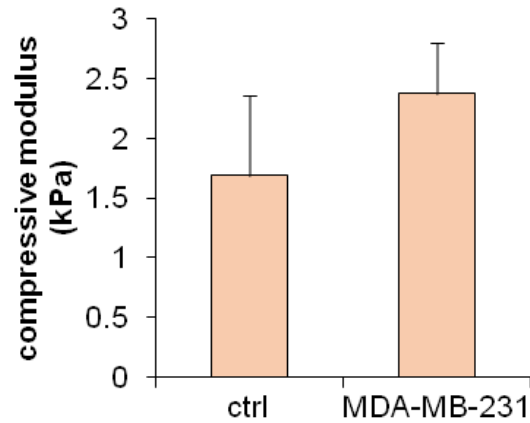


Figure 27. Average compressive modulus (kPa) for uncellularized scaffolds (ctrl) or for scaffolds decellularized after a 10-day culture with MDA-MB-231. Data are mean \pm SE.

These differences between control scaffolds and scaffolds in contact with MDA-MB-231 were similar to that observed with the prototype low-force compressive device, although the absolute compressive modulus values determined by DMA analysis resulted markedly lower than that determined with the prototype device. The ability of MDA-MB-231 to induce an increase in the stiffness of the scaffold was confirmed.

5.7 Collagen scaffold remodeling by breast cancer cells

After 10 days of culture within the scaffold, MCF-7 and MDA-MB-231 altered the structural micro- and macro- characteristics of the collagen matrix. A significant decrease in the scaffold swelling property was produced by both cell lines with respect to uncellularized samples ($p= 0.022$ for MCF-7 and $p= 0.042$ for MDA-MB-231) (**Figure 28a**). The average porosity was also reduced, although the data were not statistically significant (**Figure 28b**). Both cell lines decreased the mean pore area of the scaffold, but

the decrease produced by MDA-MB-231 was higher compared to that of MCF-7 ($p=0.002$ for MDA-MB-231) (Figure 28c).

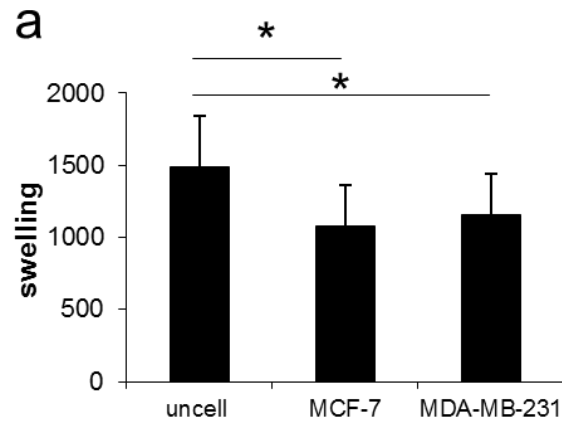


Figure 28. (a) Swelling property of the collagen scaffolds comparing samples without cells (uncell) and samples decellularized after a 10-day culture with MCF-7 or with MDA-MB-231.

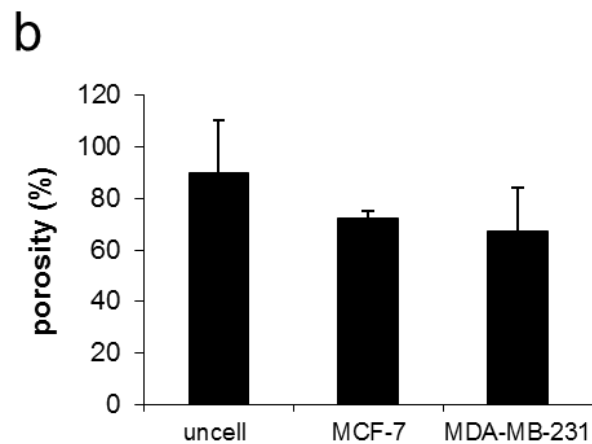


Figure 28. (b) Average porosity (%) of the collagen scaffolds comparing samples without cells (uncell) and samples decellularized after a 10-day culture with MCF-7 or with MDA-MB-231.

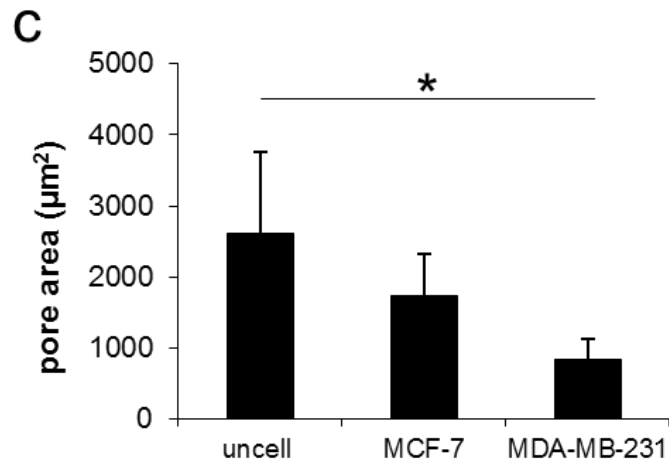


Figure 28. (c) Average pore area of the collagen scaffolds comparing samples without cells (uncell) and samples decellularized after a 10-day culture with MCF-7 or with MDA-MB-231.

SEM analysis showed the presence of a rough and irregular matrix over the scaffold surface detected after MCF-7 and MDA-MB-231 culture, while uncellularized samples displayed a smooth and regular surface (**Figure 29**).

Collagen quantification by picosirius red staining showed that the two cell lines did not increase the collagen content of the scaffold. On the contrary, collagen percentage area resulted significantly lower in scaffolds cultured with MCF-7 than in uncellularized samples (**Figure 30**). This result suggests that also matrix proteins other than collagen were deposited by the two cell lines.

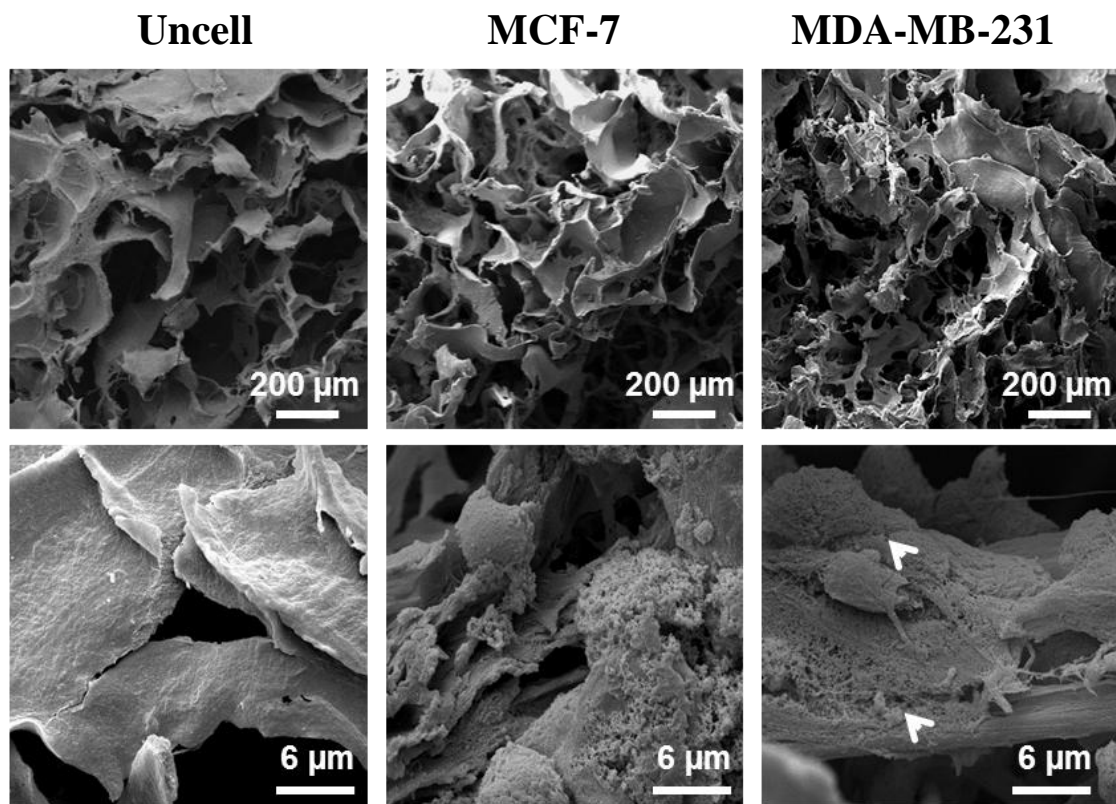


Figure 29. SEM analysis at different magnifications of the scaffolds without cells (uncell) and decellularized after a 10-day culture with MCF-7 or with MDA-MB-231. Of note: the decellularization process was performed also on empty scaffolds in order to avoid any contribution of this process on the difference between samples without cells and samples decellularized after culture with MCF-7 or MDA-MB-231; the decellularization process affected the scaffold structure, as detected at SEM analysis.

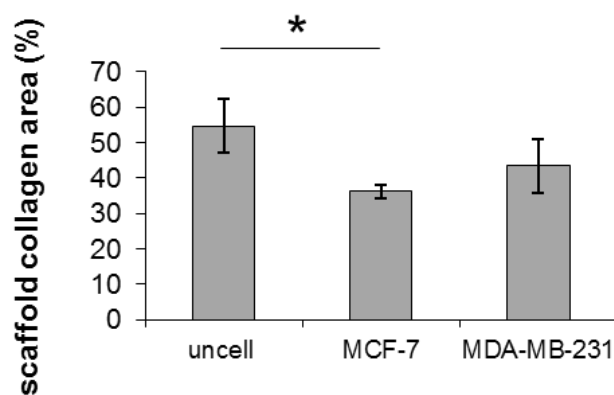
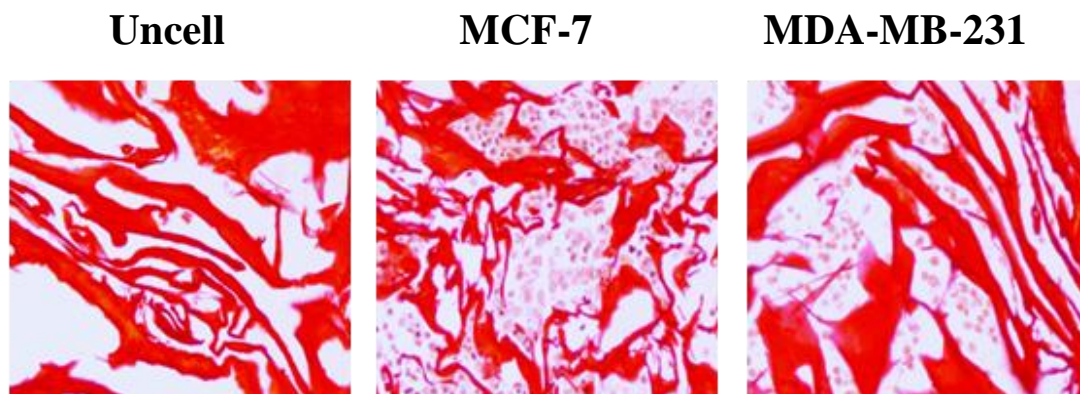


Figure 30. Picrosirius red staining of paraffin-embedded scaffolds without cells (uncell) and scaffolds decellularized after a 10-day culture with MCF-7 or with MDA-MB-231, with quantification of the mean percentage of collagen to total area. Data are mean \pm SE. * $p < 0.05$.

The matrix architecture in the scaffold was markedly different between sample uncellularized and sample cultured with MCF-7 or MDA-MB-231 as detected by Masson's thricrome staining. In particular, the matrix appeared more organized, highly packed and with linear collagen fibers (arrowhead) in the presence of MDA-MB-231. While uncellularized scaffolds and scaffolds cultured with MCF-7 display a more dispersed and disorganized matrix (**Figure 31**).

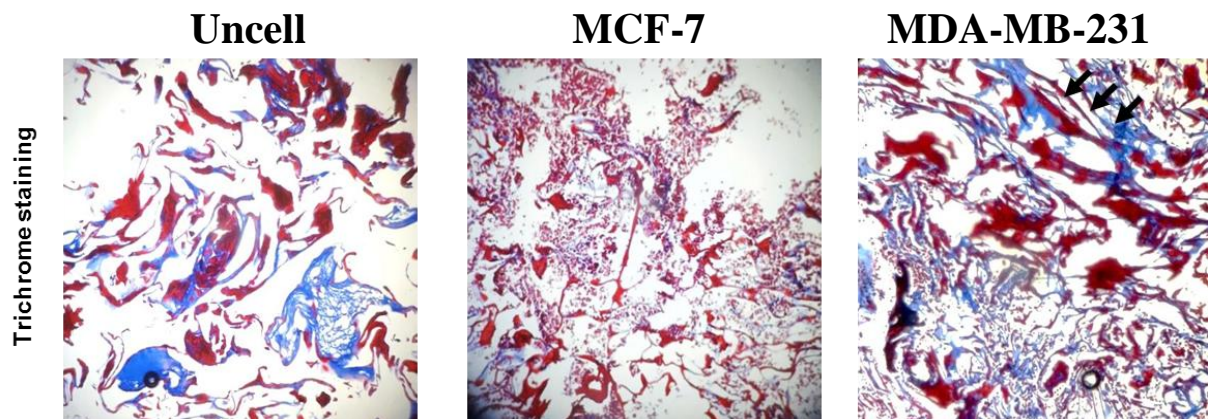


Figure 31. Trichrome staining of paraffin-embedded scaffolds without cells (uncell) and decellularized after a 10-day culture with MCF-7 or with MDA-MB-231.

5.8 LOX inhibition impairs MDA-MB-231 ability to increase collagen stiffness

Treatment with BAPN did not affect proliferation of MDA-MB-231, as the survival percentage of treated cells was similar to that of untreated controls (**Figure 32a**). In the presence of LOX inhibition the ability of MDA-MB-231 to increase the stiffness of the collagen scaffold was reduced: uncellularized samples displayed an average compressive modulus of 55.5 ± 2.6 kPa, while samples decellularized after MDA-MB-231 culture with BAPN treatment showed an average compressive modulus of 58.1 ± 5.2 kPa (**Figure 32b**). Scaffold compressive modulus increased by 8.9%, in contrast to the increase observed without LOX inhibition (23%) (**Figure 32c**).

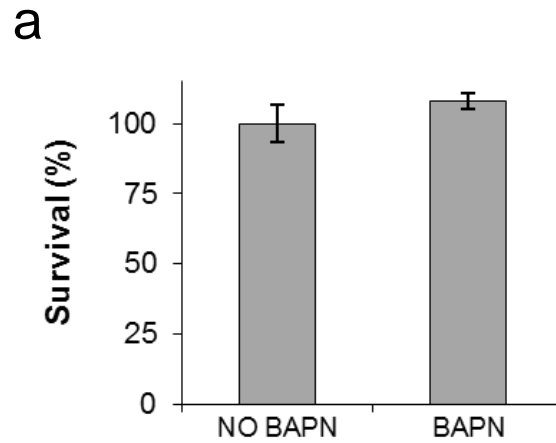


Figure 32. (a) Survival percentages of MDA-MB-231 cultured within the scaffold in the absence (NO BAPN) or presence (BAPN) of a LOX inhibitor. Data are mean \pm SE.

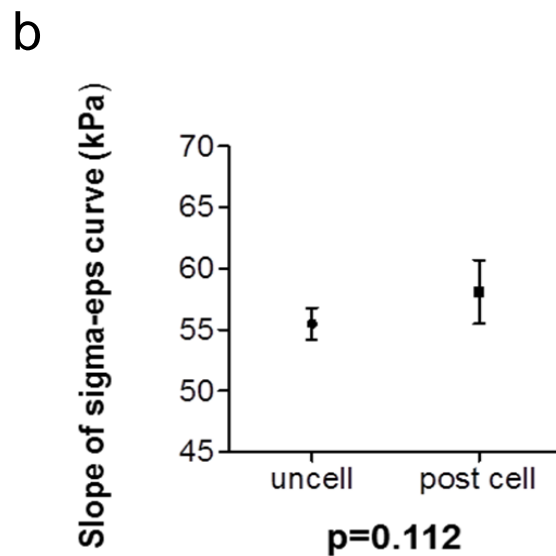


Figure 32. (b) Average slope of the sigma-eps curve (kPa) for uncellularized scaffolds or for scaffolds decellularized after a 10-day culture with MDA-MB-231 in the presence of LOX inhibition. Data are mean \pm SE.

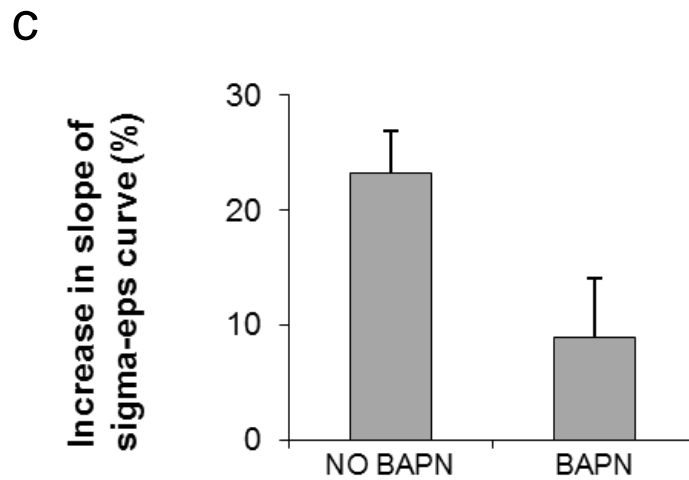


Figure 32. (c) Percentage increase in the slope of the sigma-eps curve for scaffolds decellularized after a 10-day culture with MDA-MB-231 in the presence or absence of LOX inhibition (BAPN and NO BAPN, respectively) with respect to uncellularized scaffolds. Data are mean \pm SE.

5.9 Atomic Force Microscopy analysis of single collagen fibers

We used a surface mapping technique called PeakForce QNM AFM in order to evaluate the nanomechanical features of the fibers of uncellularized control scaffolds and scaffolds after a 10 day culture with MDA-MB-231. AFM images of the collagen fibers were collected from different samples and at random spot surface sampling (**Figure 33a and b**).

a

ctrl

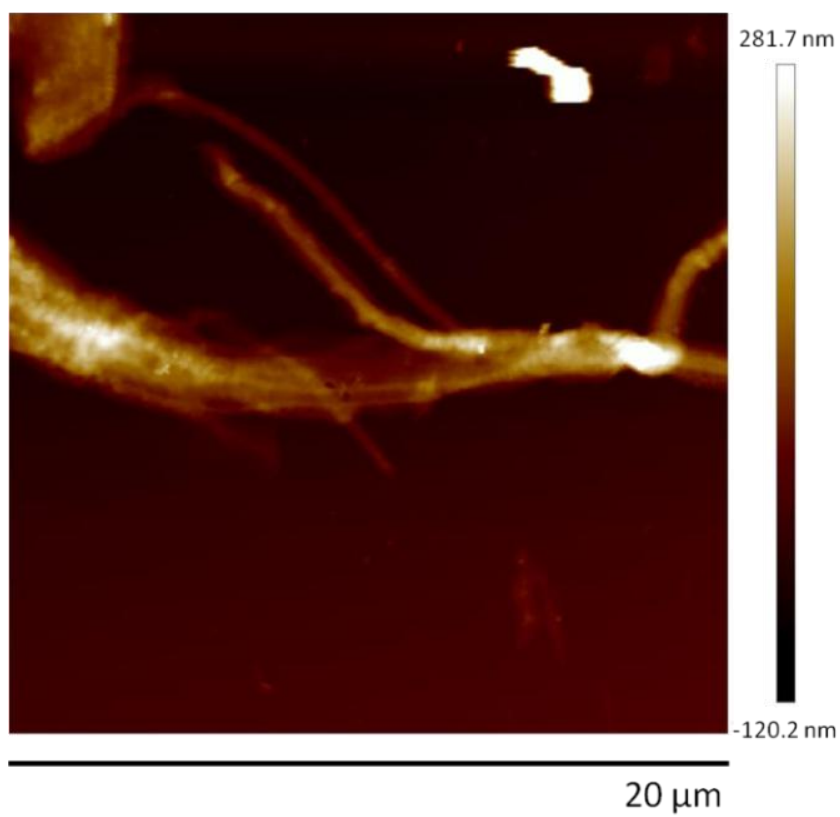


Figure 33. (a) Representative images of a collagen fiber taken from an uncellularized scaffold at the Atomic Force Microscope.

a

MDA-MB-231

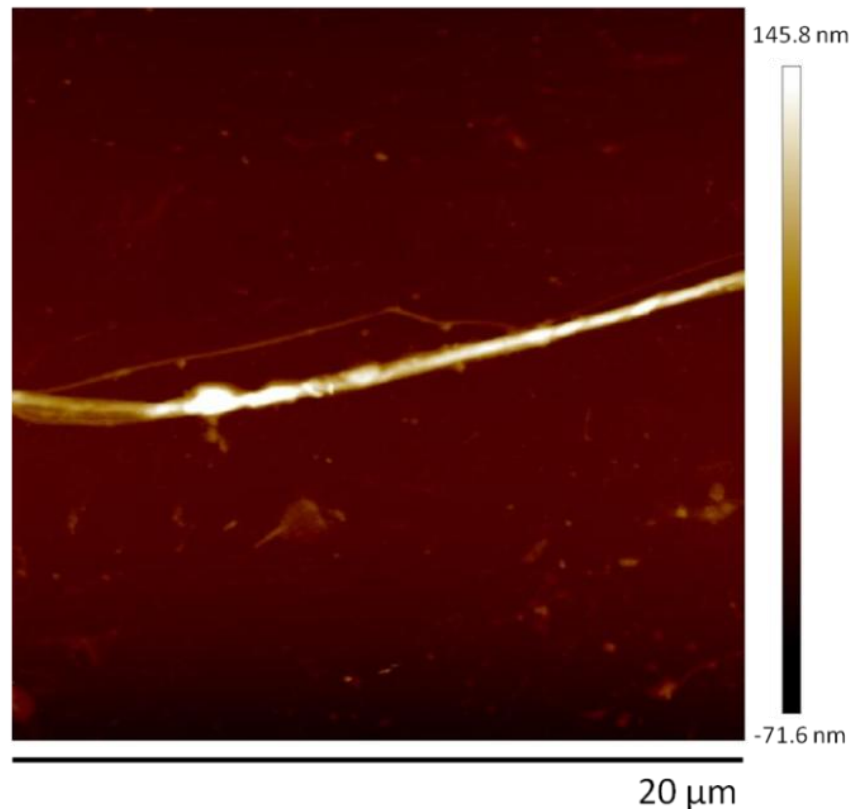


Figure 33. (b) Representative images of a collagen fiber taken from a scaffold decellularized after a 10-day culture with MDA-MB-231 at the Atomic Force Microscope.

No significant differences were observed between the Young's modulus of fibers taken from control scaffolds, which was 1.08 ± 0.24 GPa, compared to the Young's modulus of fibers taken from scaffolds decellularized after the culture with MDA-MB-231, which was $1.1 \text{ GPa} \pm 0.05$ (**Figure 34**). This results could be explained by the functional correlation found between the ability of MDA-MB-231 to increase the scaffold's stiffness and the activity of LOX. The collagen cross-linking mediated by this enzyme involve inter-fibers bonds that are probably lost with this type of analysis that allow for the determination of the strength of single fibers.

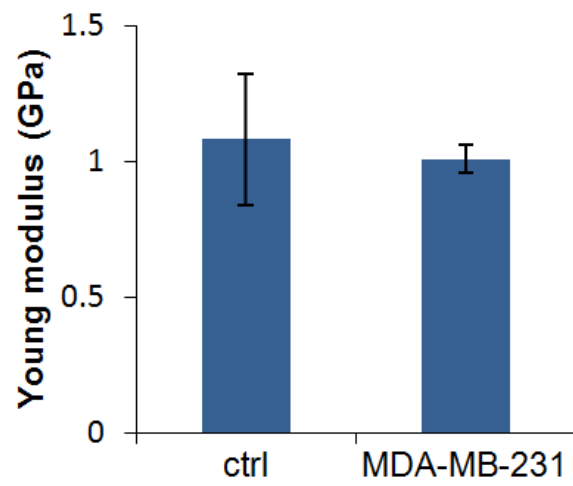


Figure 34. Young's modulus of fibers taken from uncellularized scaffolds (ctrl) compared to fibers taken from scaffolds decellularized after the culture with MDA-MB-231.

6. Discussion

Physical sciences and engineering have introduced novel perspectives into the study of cancer through model systems, tools, and metrics that enable a higher integration of basic science observations with clinical data (Cassereau et al., 2015; Paszek et al., 2005 and Wozniak et al., 2012). Empirical studies that employ complex *in vitro* and *in vivo* model systems to assess and control cell behavior and/or mathematical models that simulate molecular and cellular processes (Carey SP et al., 2012) have contributed to the identification of several complex mechanisms that drive processes during cancer progression including tumor growth, angiogenesis, and metastasis. In particular, the use of three-dimensional culturing models has recently open the window to a new era for cancer research. The generation of 3D cancer models with various technologies (i.e. the use of spheroids, bio-printing, or assembly) has allowed to recapitulate and control defined physical and biochemical factors while culturing cancer cells mimicking the tumor native microenvironment (Asghar et al., 2015). These strategically-designed approaches are increasingly used to study mechanisms of disease progression or drug effect in cancer.

These approaches are now implemented with the use of numerous kinds of biomaterials such as hydrogels, scaffolds, and basement membrane extracts. Three-dimensional models based on materials with elevated mimicking of *in vivo* tissue properties offer researcher the ideal tool to improve the standard culturing systems, i) allowing cancer cells to growth in native microenvironmental conditions and ii) providing unique platform to study bio-physical aspects, that cannot be included into standard monolayer or scaffold-free cultures. As an example, 3D scaffolds that enable the tuning of matrix microstructure, stiffness and composition offer an *in vitro* experimental model to study the effects exerted by these

physical and mechanical parameters on the behavior of cancer cells (Insua-Rodriguez et al., 2016; Levental et al., 2009 and Shawn et al., 2012).

It is known, indeed, that a dynamic mechanical interaction subsists between cancer cells and the surrounding ECM environment and governs essential tumor processes (Kumar et al., 2009). The mechanical characteristics of tumors and tumor cells are predictive of the disease clinical behavior (Plodinec et al., 2012; Xu et al., 2012) and mechanical signaling from the ECM influence the tumor phenotypes (Paszek et al., 2005; Tan et al., 2014 and Ulrich et al., 2009). Thus, investigating the cancer mechanobiology represents a great opportunity to achieve a better understanding of the disease and to identify novel possible therapeutic targets or prognostic biomarkers.

In this study we have utilized type I collagen scaffolds as an *in vitro* 3D biomimetic model to study the interaction occurring between MDA-MB-231 or MCF-7 breast cancer cells, known for having different clinical aggressiveness (Kolliday et al., 2011), and the surrounding ECM. Towards this end, our collagen scaffold seems a model of choice, as it (i) resembles the main component of the ECM; (ii) can be easily fabricated; (iii) and each feature can be tuned (e.g. structure, pore size, porosity, wettability, degradation) (Minardi et al., 2014).

The pore sizes of the collagen scaffolds ranged from 150 to 300 μm , which is sufficient for exchange of oxygen and nutrients, and suitable for cell attachment (Chen et al., 2012). We first demonstrated that our collagen scaffolds retained the typical D- periodicity of native collagen tissues. Collagen molecules are packed in a quarter staggered fashion which gives rise to a repeating banding pattern, the so-called D-periodicity or D-band, of about 67nm (Fratzl et al., 2008). It has been found that the transverse D-banding periodic pattern is a key player of collagen fiber mechanical properties, while it has been correlated with pathological conditions and it is believed to play a significant role in cell-collagen interactions (Grant et al., 2012). As an example, a strong correlation between the

orientation of D-band and cell elongation has been reported on two-dimensional collagen surfaces (Poole et al., 2005).

We next proved, in a xenograft orthotopic murine model, that the ECM characteristics of breast tumors are related to the phenotypes and the aggressiveness of cancer cells. We showed that *in vivo* tumors generated by MDA-MB-231 cells, belonging to the more aggressive basal-like subtype (corresponding to TNBC), were characterized by a distinct ECM signature compared to tumors generated by MCF-7. In particular, MDA-MB-231 tumors were characterized by elevated collagen content and a high degree of collagen linearization. Furthermore, in tumors generated by MDA-MB-231 we found a higher expression of the collagen cross-linking enzyme LOX. Increased LOX levels and tumor stiffness have been associated with progression (Butcher et al., 2009; Levental et al., 2009; Oskarsson et al., 2013 and Payne et al., 2007) and local invasion via oriented cell migration on aligned collagen fibers (Provenzano et al., 2006). Moreover, the elevated expression of fibrillar collagens has been linked to the invasive and aggressive behavior of breast tumors (Zaman et al., 2006). Similar changes have been described by Acerbi and colleagues in specific subtypes of breast cancers. The authors found that the stroma at the invasive region of basal-like and HER2 tumor subtypes was the most heterogeneous and the stiffest when compared to the less aggressive luminal A and B subtypes (Acerbi et al., 2015).

We next investigated the phenotypes and behavior of breast cancer cells when growing in collagen-based 3D scaffolds. Both cell lines within the scaffolds preserved their specific traits. Weakly aggressive MCF-7 cells displayed an epithelial-like morphology and a high expression of the E-cadherin epithelial marker. Conversely, MDA-MB-231 showed an infiltrating and mesenchymal phenotype with lower E-cadherin expression and high levels of vimentin. Loss of E-cadherin is a key step in the epithelial to mesenchymal transition (EMT) process and has been implicated in cancer progression and metastasis (Beavon et

al., 2000; Onder et al., 2008). On the other hand, vimentin expression fosters a number of cellular changes involved in the acquisition of a mesenchymal trait, including increased cell motility (Mendez et al., 2010). The 3D environmental conditions stimulated different responses between MDA-MB-231 and MCF-7. Consistently with the more aggressive phenotype, MDA-MB-231 cells migrated radially toward the rim of the scaffold assuming a migratory pattern called “Indian filing”. Conversely, this behavior was not observed for less invasive MCF-7 cells.

Drug sensitivity was also affected by culturing breast cancer cells in this 3D model. In particular, the ER⁺ luminal A cell lines proved little responsiveness to Doxorubicin in the 3D settings, while sensitivity resulted much higher in monolayer culture. Consistently, there is emerging clinical evidence that indicates possible lack of benefit from anthracycline chemotherapy in patient with ER⁺ luminal A breast tumors with non aggressive features (Kathy. et al., 2011; Barrios et al., 2009).

In order to study the mechanical interaction of the breast cancer cells with the collagen matrix we first evaluated the compression-dependent viscoelastic properties of the scaffolds. To this aim we developed a low-force compression testing device: the instrument consisted of a cylindrical piston to indent the samples with known loadings, and a comparator for detecting the piston displacement to a determined load. Using this prototype device, we were able to show that MDA-MB-231 cancer cells, when cultured for 10 day on the scaffolds, produced a significant increase in the macroscopic stiffness of collagen samples (the average slope of the sigma-epsilon curve increased from 46.9 ± 2.7 kPa to 57.9 ± 3.6 kPa). Conversely, MCF-7 did not affect this property.

These data were confirmed by the use of Dynamic Mechanical Analysis, a standard technique for measuring the mechanical properties of biomaterials. In compression, the scaffolds showed three characteristic deformation stages, as it was already been describe

for similar collagen materials (**Figure 35**): the first stage was the linear elastic stage (dominated by the bending of pore edges), followed by a stress plateau (dominated by pore wall buckling) and a stage of densification (dominated by pore collapse throughout the scaffold) (Chen et al., 2012). The slopes of the initial linear stages on the curves represent the compressive modulus.

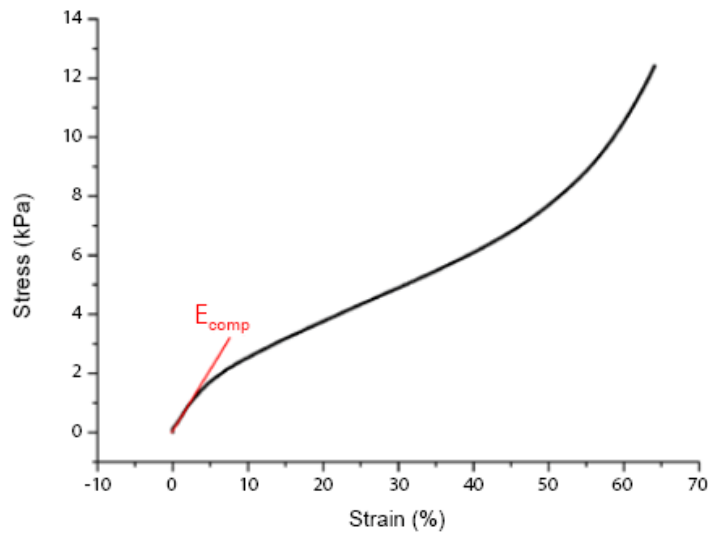


Figure 35. Example of unidirectional compression stress-strain curves of collagen scaffolds determined with a DMA instrument (Chen et al., 2012).

The differences between control scaffolds and scaffolds in contact with MDA-MB-231 assessed by DMA were similar to those observed with the prototype low-force compressive device. Although the modulus values determined by the DMA analysis resulted markedly lower than those determined with the prototype device (1.7 ± 0.7 kPa versus 46.9 ± 2.7 kPa as assessed by DMA or by the low-force testing device, respectively), the ability of MDA-MB-231 to increase the stiffness of the scaffold was confirmed by both techniques.

We next characterized the structural remodeling induced by cancer cells on the collagen matrix. We showed that both cell lines induced a decrease in the scaffold swelling property and pore area, probably as a result of the deposition of new matrix. The decrease in the swelling property and pore size can lead to an increase in the stiffness of collagen polymers (Grover et al., 2012). Although both cell lines affected these two parameters, only MDA-MB-231 were able to modify the scaffold stiffness. With a deeper investigation, we showed that MDA-MB-231 were able to alter the scaffold architecture producing a more organized and packed matrix, characterized by the presence of linear collagen fibers. In addition, this cell line, when cultured on the scaffold, expressed high levels of the collagen-crosslinking enzyme LOX (consistently with what observed *in vivo*). Conversely, MCF-7 expressed lower levels of LOX and were unable to significantly modify the architecture of the matrix. Collagen crosslinking is related to its stiffness properties (Buehler et al., 2006) and is, to a large extent, enzymatically catalyzed by the lysyl oxidase family (Payne et al., 2007). When LOX activity was blocked, MDA-MB-231 ability to alter the scaffold stiffness was impaired, providing a causal correlation between LOX-mediated collagen crosslinking and the observed stiffness increase.

This finding has particular relevance, since increased LOX expression and tumor stiffness have been associated with progression (Butcher et al., 2009; Levental et al., 2009; Oskarsson et al., 2013) and local invasion via oriented cell migration along aligned collagen fibers (Egeblad et al., 2010; Provenzano et al., 2006). LOX has also been found associated with breast cancer prognosis. Patients with high LOX-expressing tumors have poor overall survival, and inhibition of LOX has been demonstrated to eliminate metastases in mice. Recent research has also shown that overexpression of LOX is crucial to promote metastasis in several cancers, including breast cancer (Erler et al., 2006; Erler et al., 2009 and Kirschmann et al., 2002), non-small cell lung cancer (Shi et al., 2012) and colorectal cancer (Baker et al. 2011).

MDA-MB-231 seemed also to display the ability of collagen internalization which constitutes an important mechanism for ECM turnover and remodeling (Curino et al., 2005). This process has been correlated with breast cancer progression and was first described in tumor-associated stromal cells which are able to internalize and degrade collagen through the uPARAP/Endo180 receptor (Engelholm et al., 2003). Recent findings have shown that the collagen receptor Endo180 is also expressed in basal-like breast tumor cells (Wienke et al., 2007) and that some cancer cells have the ability to internalize collagen (Huijbers et al., 2010; Ikenaga et al. 2012). In addition, it has been found that EMT fosters this pathway, leading prostate cancer cells with a mesenchymal phenotype to develop an enhanced ability to internalize collagen (Ikenaga et al., 2012).

Finally, we studied through Atomic Force Microscopy the mechanical micro-properties of single collagen fibers, comparing fibers taken from uncellularized scaffolds and fibers taken from scaffolds cultured with MDA-MB-231. No significant differences were observed between the Young's modulus of collagen fibers from control scaffolds compared to fibers from scaffolds after the culture with breast cancer cells. This results is explained by the functional correlation found between the increase in the scaffold's stiffness produced by MDA-MB-231 and the activity of LOX. It is know that the collagen cross-linking mediated by this enzyme involve inter-fibers bonds, as the substrate to generate cross-links are collagen fibrils in a quarter staggered array (Kagan and Li, 2003). When analyzing the mechanical properties at the single fiber level this type of interactions are probably lost and, thus, no differences are observed between control fibers and fibers in contact with cancer cells. The results obtained were consistent with other previously reported data on the Young's modulus of collagen fibers determined through AFM (Wenger et al., 2007; Liu et al., 2013; Minardi et al., 2015).

Despite the fact that 3D collagen models are very promising, their characterization can be complicated. Unlike hard scaffolds, the mechanical properties of soft materials are difficult to be characterized due to their fragility. They usually can only tolerate nN stresses, making them difficult to measure. Although AFM is a surface characterization technique, it offer a significant tool for imaging and characterization of the micro-structural and mechanical properties of these 3D materials (Stylianou, 2017 and Rettler et al., 2013) (**Figure 36**).

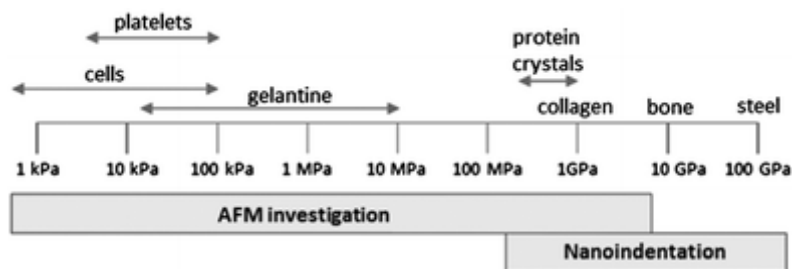


Figure 36. AFM is suitable to investigate the properties of collagen fibers (Rettler et al., 2013).

There are a number of studies where the coupling of an AFM characterization with the use of collagen materials permitted to explore macro- and micro- properties of tailored collagens and the effect of these properties on different cell types. For example, Tan et al. applied AFM imaging to investigate the surface modifications induced by the incorporation of chitosan on collagen 3D gels (Tan et al., 2010). Vicens-Zygmunt et al. used AFM to study the ribose-induced mechanical alterations and the consequent fibroblast phenotypes in collagen gels by assessing their Young's elastic modulus (Vicens-Zygmunt et al., 2015). Nam and colleagues used AFM to explore the strain stiffening of collagen gels (Nam et al., 2016). Zhu et al. recently reported a new approach for characterizing the stiffness and elastic modulus of collagen-chitosan hydrogel scaffolds

using AFM. They developed and introduce a mathematical model to determine the stiffness and the elastic modulus of a scaffold from its force curve obtained in liquid conditions and using a triangle probe to indent the samples (**Figure 37**) (Zhu et al., 2011).

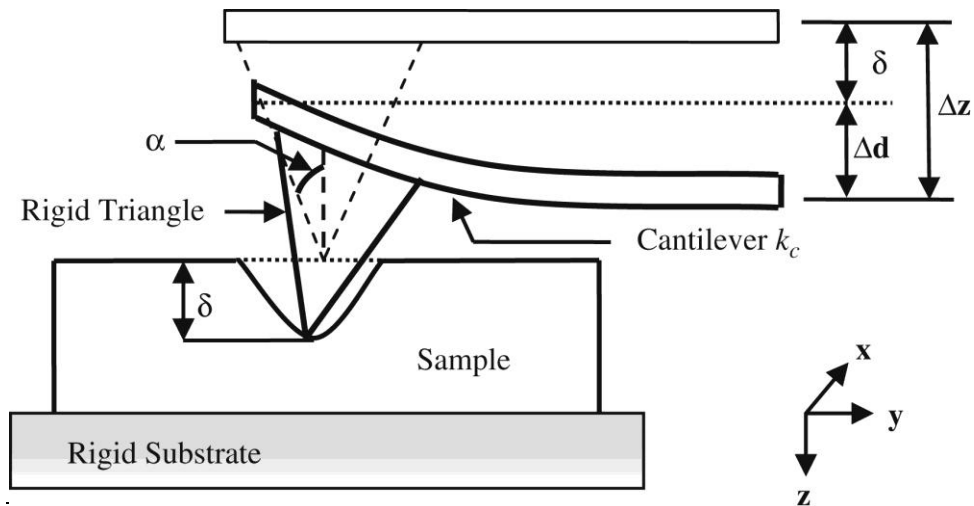


Figure 37. Schematic of indentation of a thin biological sample by a triangle probe in AFM, developed by Zhu et al.

Using this method, Zhu and colleagues were able to demonstrate that fibroblast-like cells are able to significantly increase the elastic modulus of collagen fibers. Furthermore, this method allowed the authors to efficiently determine the elastic moduli of mouse pancreas and heart samples.

Finally, van Helvert and Friedl performed AFM nanoindentation in live-cell culture in order to directly address local elasticity changes generated by moving cells on fibrillar type I collagen gels (van Helvert and Friedl, 2016).

Thus, coupling the AFM technique with the use of *in vitro* scaffold- or gel- based models offer a unique opportunity to collect qualitative or quantitative information on: i) micro-properties of soft tissue materials with diverse structure and composition; ii) forces at the single cell level; iii) matrix-cells micro-interactions.

In conclusion we provided evidence that cancer cells belonging to the aggressive basal-like subtype of breast tumors display the ability to modify the surrounding ECM and, in particular, are able to alter the mechanical properties of extracellular collagen. This process is caused by a remodeling on the matrix architecture mediated by the activity of LOX, a collagen cross-linking enzyme, highly expressed by the invasive breast cancer cell line.

7. Conclusions and future perspectives

Overall this work provides evidence that aggressive basal-like breast cancer cells modify the surrounding ECM and, in particular, are able to alter the architecture of extracellular collagen and increase its stiffness.

These findings were obtained by coupling an experimental *in vitro* cell culture model, based on 3D collagen scaffolds, with a number of different methodologies to characterize the composition and the structural and mechanical macro- and micro- properties of soft biomaterials. The remodeling produced in the collagen scaffolds by aggressive cancer cells is consistent with the characteristics observed in the ECM of *in vivo* tumors and with previous findings on the ECM properties of basal-like breast cancers (i.e. Acerbi et al., 2015). These observations confirm that our model might constitute a relevant and informative experimental system to further address the mechanobiology of cell-ECM interaction.

In particular, one of the future application of this model will be the study of the influence of scaffold stiffness on the phenotype and behavior of cancer cells. The scaffold stiffness will be modified by increasing the concentration of the crosslinking reagent during the chemical synthesis of the samples. The cross-link conditions will be then correlated with the compressive modulus assessed with the prototype device, and the impact of these properties on the cellular and molecular phenotypes of cancer cells, as well as on their drug sensitiveness, will be evaluated.

The use of collagen as the main component of our scaffold will allow for the evolution of our system into progressively complex models as: (i) it is the main component of the ECM of every tissue of the body; (ii) its abundance of functional groups (carboxylic and aminic groups), will enable for the introduction of other components of

the ECM (e.g. proteins, carbohydrates), bioactive factors and stromal cells into the system to engineer more sophisticated tissue-specific tumor niches; (iii) the possibility to create complex geometries and intra-scaffold compartments, to mimic complex tissues (Minardi et al., 2014); (iv) the changes in its concentration, type and crosslinking can lead to large effects on the mechanical properties of the tissue.

8. References

1. Acerbi I, et al. Human breast cancer invasion and aggression correlates with ECM stiffening and immune cell infiltration. *Integr Biol (Camb)*. 7:1120-1134, 2015.
2. Allison DP, Mortensen NP, Sullivan CJ, Doktycz MJ. Atomic force microscopy of biological samples. *Wiley Interdiscip Rev Nanomed Nanobiotechnol*. 2010 Nov-Dec;2(6):618-34.
3. Asghar W, El Assal R, Shafiee H, Pitteri S, Paulmurugan R, Demirci U. Engineering cancer microenvironments for in vitro 3-D tumor models. *Mater Today (Kidlington)*. 2015 Dec;18(10):539-553.
4. Baker AM, et al. The role of lysyl oxidase in SRC-dependent proliferation and metastasis of colorectal cancer. *Journal of the National Cancer Institute*. 2011; 103 (5): 407–24.
5. Barone AC, et al. Calibration issues for nanoindentation experiments: direct atomic force microscopy measurements and indirect methods. *Microsc. Res. Technol.*, 73 (2010), pp. 996–1004
6. Barrios CH, et al. What is the role of chemotherapy in estrogen receptor-positive, advanced breast cancer? *Ann Oncol*. 2009;20, 1157-1162.
7. Beavon IR. The E-cadherin- catenin complex in tumour metastasis: structure, function and regulation. *Eur J Cancer*. 2000;(13 Spec No):1607-20.
8. Beer F, et al. *Mechanics of Materials*. 6th edition. McGraw-Hill Publ., 2011.
9. Bergamaschi A, et al. Extracellular matrix signature identifies breast cancer subgroups with different clinical outcome. *J Pathol*. 214:357-67, 2008.
10. Binnig G, Quate CF, Gerber C. Atomic force microscope. *Phys Rev Lett*. 1986 Mar 3;56(9):930-933.
11. Bondareva A, et al. The Lysyl Oxidase Inhibitor, β -Aminopropionitrile, Diminishes the Metastatic Colonization Potential of Circulating Breast Cancer Cells. *PLoS ONE*. 4(5): e5620, 2009.
12. Bonnans C., et al. Remodelling the extracellular matrix in development and disease. *Nat Rev Mol Cell Biol*. 15:786-801, 2014.
13. Buehler MJ. Nature designs tough collagen: explaining the nanostructure of collagen fibrils. *Proc Natl Acad Sci U S A*. 103:12285-12290, 2006.

14. Butcher DT, et al. A tense situation: forcing tumour progression. *Nat Rev Cancer*. 9:108-122, 2009.
15. Carey LA, et al. The triple negative paradox: primary tumor chemosensitivity of breast cancer subtypes. *Clin Cancer Res*. 2007; 13: 2329–34.
16. Carey SP, et al. Reinhart-King. Mechanobiology of tumor invasion: engineering meets oncology. *Crit Rev Oncol Hematol*. 83:170-183, 2012.
17. Carey SP, Kraning-Rush CM, Williams RM, Reinhart-King CA. Biophysical control of invasive tumor cell behavior by extracellular matrix microarchitecture. *Biomaterials*. 2012;33(16):4157-4165. doi:10.1016/j.biomaterials.2012.02.029.
18. Cassereau L, et al. A 3D tension bioreactor platform to study the interplay between ECM stiffness and tumor phenotype. *J Biotechnol*. 193:66-69, 2015.
19. Cavo M, et al. Microenvironment complexity and matrix stiffness regulate breast cancer cell activity in a 3D in vitro model. *Scientific reports* 6 (2016).
20. Chauhan VP, Boucher Y, Ferrone CR, Roberge S, Martin JD, Stylianopoulos T, Bardeesy N, DePinho RA, Padera TP, Munn LL, Jain RK. Compression of pancreatic tumor blood vessels by hyaluronan is caused by solid stress and not interstitial fluid pressure. *Cancer Cell*. 2014 Jul 14;26(1):14-5.
21. Chen Q, Bruyneel A, Clarke K, Carr C, Czernuszka J (2012) Collagen- Based Scaffolds for Potential Application of Heart Valve Tissue Engineering. *J Tissue Sci Eng* S11:003
22. Cisneros DA, Friedrichs J, Taubenberger A, Franz CM, Muller DJ. Creating ultrathin nanoscopic collagen matrices for biological and biotechnological applications. *Small*. 2007 Jun;3(6):956-63.
23. Clifford CA, Seah M.P. Modeling of nanomechanical nanoindentation measurements using an AFM or nanoindenter for compliant layers on stiffer substrates. *Nanotechnology*, 17 (2006), pp. 5283–5292
24. Cox TR, et al. "The hypoxic cancer secretome induces pre-metastatic bone lesions through lysyl oxidase." *Nature* 522.7554 (2015): 106-110.
25. Curino AC, et al. Intracellular collagen degradation mediated by uPARAP/Endo180 is a major pathway of extracellular matrix turnover during malignancy. *J Cell Biol*. 169:977-985, 2005.

26. Cuzick J, et al. Tamoxifen-induced reduction in mammographic density and breast cancer risk reduction: a nested case-control study. *J Natl Cancer Inst.* 103:744-752, 2011.
27. Darling EM, et al. A thin-layer model for viscoelastic, stress-relaxation testing of cells using atomic force microscopy: do cell properties reflect metastatic potential? *Biophys. J.*, 92 (2007), pp. 1784–1791
28. Dent S, et al. HER2-targeted therapy in breast cancer: a systematic review of neoadjuvant trials. *Cancer Treat Rev.* 2013; 39: 622–31.
29. Derjaguin BV, Müller VM, Toporov YP. Effect of contact deformations on adhesion of particles. *Journal of Colloid and Interface Science.* 1975;53:314-326.
30. Desantis C, et al. *Breast Cancer Statistics, 2013.* 2013; 00: 1–11.
31. Doube M, et al. Combined nanoindentation testing and scanning electron microscopy of bone and articular calcified cartilage in an equine fracture predilection site. *Eur. Cell Mater.*, 19 (2010), pp. 242–251
32. Du Fort CC, et al. Weaver. Balancing forces: architectural control of mechanotransduction. *Nat Rev Mol Cell Biol.* 12:308-319, 2011.
33. Dvorak HF, et al. Tumor microenvironment and progression. *J Surg Oncol.* 103:468-474, 2011.
34. Edmondson D, et al. "Design and evaluation of a nanoscale differential tensile test device for nanofibers. *Applied Physics Letters* 94.10 (2009): 103101.
35. Egeblad M, et al. Dynamic interplay between the collagen scaffold and tumor evolution. *Curr Opin Cell Biol.* 2010;22, 697-706.
36. Elsamany S, et al. Prognostic value of mammographic breast density in patients with metastatic breast cancer. *Med Oncol.* 31:96, 2014.
37. Engelholm LH, et al. uPARAP/Endo180 is essential for cellular uptake of collagen and promotes fibroblast collagen adhesion. *J Cell Biol.* 2003;160(7):1009-15.
38. Engler A J, et al. Discher. Matrix elasticity directs stem cell lineage specification. *Cell.* 126:677-689, 2006.
39. Erler JT, et al. Hypoxia-induced lysyl oxidase is a critical mediator of bone marrow cell recruitment to form the premetastatic niche. *Cancer Cell.* 2009;15:35–44.

40. Erler JT, et al. Lysyl oxidase is essential for hypoxia-induced metastasis. *Nature*. 2006;440:1222–6.
41. Erler JT, Giaccia A.J. Lysyl oxidase mediates hypoxic control of metastasis. *Cancer Res*. 2006;66:10238–41.
42. Fang M, et al. Collagen as a double-edged sword in tumor progression. *Tumor Biology* 35.4 (2014): 2871-2882.
43. Fenner J, et al. Macroscopic stiffness of breast tumors predicts metastasis. *Sci Rep*. 4:5512, 2014.
44. Ferlay J, Soerjomataram I, Ervik M, Dikshit R, Eser S, Mathers C, et al. GLOBOCAN 2012 v1.0, Cancer Incidence and Mortality Worldwide: IARC CancerBase No. 11; 2012
45. Florczyk SJ, et al. "Porous chitosan-hyaluronic acid scaffolds as a mimic of glioblastoma microenvironment ECM." *Biomaterials* 34.38 (2013): 10143-10150.
46. Frantz C, Stewart KM, Weaver VM. The extracellular matrix at a glance. *J Cell Sci*. 2010 Dec 15;123(24):4195-200.
47. Fratzl P, *Collagen Structure and Mechanics*, Springer, New York, NY, USA, 2008
48. Ghosh S, Gutierrez V, Fernández C, Rodriguez-Perez MA, Viana JC, Reis RL, Mano JF. Dynamic mechanical behavior of starch-based scaffolds in dry and physiologically simulated conditions: effect of porosity and pore size. *Acta Biomater*. 2008 Jul;4(4):950-9.
49. Gonzalez LO, et al. Expression of metalloproteases and their inhibitors by tumor and stromal cells in ductal carcinoma in situ of the breast and their relationship with microinvasive events. *J Cancer Res Clin Oncol*. 2010;136:1313–21.
50. Grant CA, Phillips MA, and Thomson NH. "Dynamic mechanical analysis of collagen fibrils at the nanoscale," *Journal of the Mechanical Behavior of Biomedical Materials*, vol. 5, no. 1, pp. 165–170, 2012
51. Grover CN, Cameron RE, Best SM. Investigating the morphological, mechanical and degradation properties of scaffolds comprising collagen, gelatin and elastin for use in soft tissue engineering. *J Mech Behav Biomed Mater*. 2012 Jun;10:62-74.
52. Hertz H. *Über die Berührung fester elastischer Körper*. *Journal für die Reine und Angewandte Mathematik*. 1881;92:156-171
53. Hoch RV, et al. GATA-3 is expressed in association with estrogen receptor in breast cancer. *Int J Cancer*. 1999; 84: 122–8.

54. Hoffman BD, et al. Dynamic molecular processes mediate cellular mechanotransduction. *Nature*. 2011;475:316–23.
55. Holliday DL, and Speirs, V. Choosing the right cell line for breast cancer research. *Breast Cancer Res*. 13:215, 2011.
56. Hynes RO. Extracellular matrix: not just pretty fibrils. *Science (New York, NY)*. 2009;326(5957):1216-1219.
57. Hudis CA, Gianni L. Triple-negative breast cancer: an unmet medical need. *Oncologist*. 2011; 16: 1–11.
58. Huijbers IJ, et al. A role for fibrillar collagen deposition and the collagen internalization receptor endo180 in glioma invasion. *PLoS One*. 5:e9808, 2010.
59. Hulmes DJS. (2008) in *Collagen, Collagen diversity, synthesis and assembly*, ed Fratzl P. (Springer, London), pp 15–47
60. Ikenaga N, et al. Pancreatic cancer cells enhance the ability of collagen internalization during epithelial-mesenchymal transition. *PLoS One*. 2012;7(7):e40434.
61. Infanger DW, et al. Engineered culture models for studies of tumor-microenvironment interactions. *Annu Rev Biomed Eng*. 15:29-53, 2013.
62. Insua-Rodríguez J, Oskarsson T. The extracellular matrix in breast cancer. *Adv Drug Deliv Rev*. 97:41-55, 2016.
63. Janmey PA, Miller R. T. Mechanisms of mechanical signaling in development and disease. *J Cell Sci*. 124:9-18, 2011.
64. Jarvelainen H, Sainio A, Koulu M, Wight T N, Penttinen R. (2009). Extracellular matrix molecules: potential targets in pharmacotherapy. *Pharmacol. Rev*. 61, 198-223
65. Johnson KL, Kendall K, Roberts AD. Surface energy and contact of elastic solids. *Proceedings of the Royal Society of London Series A – Mathematical and Physical Science*. 1971;324:301
66. Kagan HM, Li W. Lysyl oxidase: properties, specificity, and biological roles inside and outside of the cell. *J Cell Biochem*. 2003;88:660–72
67. Kang Y, et al. A multigenic program mediating breast cancer metastasis to bone. *Cancer Cell*. 3:537-549, 2003.

68. Kathy S, et al. Prognostic and predictive value of the 21-gene recurrence score assay in a randomized trial of chemotherapy for postmenopausal, node-positive, estrogen receptor positive breast cancer. *Lancet Oncol.* 2011. Author manuscript available in PMC 16.
69. Kirschmann DA, et al. A molecular role for lysyl oxidase in breast cancer invasion. *Cancer Research.* 2002; 62 (15): 4478–83.
70. Kolářová H, Malohlava J, Tomankova KB, and Zapletalová H. (2012). Atomic force microscopy: Studying mechanical properties of a cell.
71. Kraning-Rush CM, Califano JP, Reinhart-King CA. Cellular Traction Stresses Increase with Increasing Metastatic Potential. Laird EG, ed. *PLoS ONE.* 2012;7(2):e32572. doi:10.1371/journal.pone.0032572.
72. Kumar S, Weaver VM. Mechanics, malignancy, and metastasis: the force journey of a tumor cell. *Cancer Metastasis Rev.* 28:113-127, 2009.
73. Kurland NE, Drira Z, Yadavalli VK. Measurement of nanomechanical properties of biomolecules using atomic force microscopy. *Micron.* 2012;43:116-128
74. Lamhamedi-Cherradi SE, et al. 3D tissue-engineered model of Ewing's sarcoma. *Adv Drug Deliv Rev.* 2014;15, 155-161.
75. Leitinger B. Transmembrane collagen receptors. *Annu. Rev. Cell Dev. Biol.* 2011;27:265–290.
76. Lesniak M, et al. A role for fibrillar collagen deposition and the collagen internalization receptor Endo180 in glioma invasion. *PLoS ONE.* 2010;5:e9808.
77. Levental KR, et al. Matrix crosslinking forces tumor progression by enhancing integrin signaling. *Cell.* 139:891-906, 2009.
78. Liu Y, Luo D, Kou X-X, Wang X-D, Tay F R, Sha Y-L, Gan Y-H and Zhou YH. (2013), Hierarchical Intrafibrillar Nanocarbonated Apatite Assembly Improves the Nanomechanics and Cytocompatibility of Mineralized Collagen. *Adv. Funct. Mater.*, 23: 1404–1411
79. Liverani, C, Mercatali, L, Cristofolini, L et al. Investigating the Mechanobiology of Cancer Cell–ECM Interaction Through Collagen-Based 3D Scaffolds. *Cel. Mol. Bioeng.* (2017) 10: 223.
80. Mano JF, Reis RL, Cunha AM. (2002) Dynamic Mechanical Analysis in Polymers for Medical Applications. In: Reis R.L., Cohn D. (eds) *Polymer Based Systems on*

Tissue Engineering, Replacement and Regeneration. NATO Science Series (Series II: Mathematics, Physics and Chemistry), vol 86. Springer, Dordrecht

81. Makris EA, Responde DJ, Paschos NK, Hu JC, Athanasiou KA. Developing functional musculoskeletal tissues through hypoxia and lysyl oxidase-induced collagen cross-linking. *Proc Natl Acad Sci U S A*. 2014 Nov 11;111(45):E4832-41.
82. Mendez MG, et al. Vimentin induces changes in cell shape, motility, and adhesion during the epithelial to mesenchymal transition. *FASEB J*. 24:1838-1851, 2010.
83. Mierke CT, et al. Integrin alpha5beta1 facilitates cancer cell invasion through enhanced contractile forces. *J Cell Sci*. 2011;124:369–83.
84. Miller JS, et al. Bioactive hydrogels made from step-growth derived PEG-peptide macromers. *Biomaterials*. 2010;(13), 3736–3743.
85. Minardi S, Corradetti B, Taraballi F, Sandri M, Van Eps J, Cabrera FJ, Weiner BK, Tampieri A, Tasciotti E. Evaluation of the osteoinductive potential of a bio-inspired scaffold mimicking the osteogenic niche for bone augmentation. *Biomaterials*. 2015 Sep;62:128-37.
86. Minardi S, et al. Multiscale patterning of a biomimetic scaffold integrated with composite microspheres. *Small*. 10:3943-3953, 2014.
87. Mintz MB, et al. An expression signature classifies chemotherapyresistant pediatric osteosarcoma. *Cancer Res* 2005;65:1748–1754.
88. Miroshnikova YA, et al. Engineering strategies to recapitulate epithelial morphogenesis within synthetic three-dimensional extracellular matrix with tunable mechanical properties. *Phys. Biol*. 2011; 8(2), 026013.
89. Nam S, Hu KH, Butte MJ, and Chaudhuri O. Strain enhanced stress relaxation impacts nonlinear elasticity in collagen gels. *Proceedings of the National Academy of Sciences of the United States of America*, vol. 113, no. 20, pp. 5492–5497, 2016.
90. Nilsson M, et al. Inhibition of Lysyl Oxidase and Lysyl Oxidase-Like Enzymes Has Tumour-Promoting and Tumour-Suppressing Roles in Experimental Prostate Cancer. *Sci Rep*. 6:19608, 2016.
91. Onder TT, et al. Loss of E-cadherin promotes metastasis via multiple downstream transcriptional pathways. *Cancer Res*. 2008;68(10):3645-54.

92. Oskarsson T. Extracellular matrix components in breast cancer progression and metastasis. *Breast*. 22(Suppl 2):S66-72, 2013.
93. Paszek MJ, et al. Tensional homeostasis and the malignant phenotype. *Cancer Cell*. 8:241-254, 2005.
94. Payne SL, et al. Paradoxical roles for lysyl oxidases in cancer--a prospect. *J Cell Biochem*. 101:1338-1354, 2007.
95. Pengfei L., et al. The extracellular matrix: A dynamic niche in cancer progression. *J Cell Biol*. 2012 Feb 20;196(4):395-406.
96. Perou CM, et al. Molecular portraits of human breast tumours. *Nature* 2000;406:747–752.
97. Plodinec M, et al. The nanomechanical signature of breast cancer. *Nat Nanotechnol*. 7:757-765, 2012.
98. Poole K, Khairy K, Friedrichs J et al., “Molecular-scale topographic cues induce the orientation and directional movement of fibroblasts on two-dimensional collagen surfaces,” *Journal of Molecular Biology*, vol. 349, no. 2, pp. 380–386, 2005
99. Provenzano PP, et al. Collagen reorganization at the tumor-stromal interface facilitates local invasion. *BMC Med*. 4:38, 2006.
100. Provenzano P.P., et al. Engineering Three-Dimensional Collagen Matrices to Provide Contact Guidance during 3D Cell Migration. *Current Protocols in Cell Biology*. 2010;10-17.
101. Rettler E, Hoepfner S, Sigusch BW and Schubert US. Mapping the mechanical properties of biomaterials on different length scales: depth-sensing indentation and AFM based nanoindentation. *J. Mater. Chem. B*, 2013,1, 2789-2806
102. Roeder BA, et al. Tensile mechanical properties of three-dimensional type I collagen extracellular matrices with varied microstructure. *J Biomech Eng*. 124:214-222, 2002.
103. Schedin P, Keely JP. Mammary gland ECM remodeling, stiffness, and mechanosignaling in normal development and tumor progression. *Cold Spring Harb Perspect Biol*. January; 3:a003228, 2011.
104. Schmidt S, Friedl P. (2010). Interstitial cell migration: integrin-dependent and alternative adhesion mechanisms. *Cell Tissue Res*. 339, 83-92

105. Shawn PC, et al. Biophysical control of invasive tumor cell behavior by extracellular matrix microarchitecture. *Biomaterials*. 33:4157-4165, 2012.
106. Shi W, et al. The effect of lysyl oxidase polymorphism on susceptibility and prognosis of nonsmall cell lung cancer. *Tumour Biology*. 2012;33 (6): 2379–83.
107. Siegel RL, et al. *Cancer Statistics, 2016*. 2016; 66: 7–30.
108. Sorlie T, et al. Gene expression patterns of breast carcinomas distinguish tumor subclasses with clinical implications. *Proc Natl Acad Sci U S A*. 2001; 98: 10869–74.
109. Sorlie T, et al. Gene expression patterns of breast carcinomas distinguish tumor subclasses with clinical implications. *Proc Natl Acad Sci U S A* 2001;98:10869–10874.
110. Sotiriou C, et al. Breast cancer classification and prognosis based on gene expression profiles from a population-based study. *Proc Natl Acad Sci U S A* 2003;100:10393–10398.
111. Stylianou A, Yova D. Surface nanoscale imaging of collagen thin films by Atomic Force Microscopy. *Mater Sci Eng C Mater Biol Appl*. 2013 Jul 1;33(5):2947-57.
112. Stylianou A. Atomic Force Microscopy for Collagen-Based Nanobiomaterials, *Journal of Nanomaterials*, vol. 2017, Article ID 9234627, 14 pages, 2017
113. Tan Y, et al. Matrix softness regulates plasticity of tumour-repopulating cells via H3K9 demethylation and Sox2 expression. *Nat Commun*. 5:4619, 2014.
114. Tan W, Krishnaraj R, Desai TA. Influence of chitosan on cell viability and proliferation in three dimensional collage gels. *Proceedings of the 22nd Annual International Conference of the IEEE Engineering in Medicine and Biology Society*, vol. 1502, pp. 1509–1524, Chicago, Ill, USA, July 2000.
115. Teschendorff AE, et al. An immune response gene expression module identifies a good prognosis subtype in estrogen receptor negative breast cancer. *Genome Biol* 2007;8:R157
116. Tomao F, et al. Triple-negative breast cancer: New perspectives for targeted therapies. *Onco Targets Ther*. 2015; 8: 177–93.
117. Tse JR, Engler AJ. Preparation of hydrogel substrates with tunable mechanical properties. *Curr. Protoc. Cell Biol*. 2010; Chapter 10: Unit 10.16

118. Ulrich TA, et al. The mechanical rigidity of the extracellular matrix regulates the structure, motility, and proliferation of glioma cells. *Cancer Res.* 69:4167-4174, 2009.
119. vanHelvert S and Friedl P. Strain stiffening of fibrillar collagen during individual and collective cell migration identified by AFM nanoindentation. *ACS Applied Materials & Interfaces*, vol. 8, no. 34, pp. 21946–21955, 2016
120. Van't Veer LJ, Weigelt B. Road map to metastasis. *Nature Med* 2003;9:999–1000.
121. Vicens-Zygmunt V, Estany S, Colom A, et al. Fibroblast viability and phenotypic changes within glycated stiffened three-dimensional collagen matrices,” *Respiratory Research*, vol. 16, article 82, 2015.
122. Wenger MPE, Bozec L, Horton MA, Mesquida P. Mechanical Properties of Collagen Fibrils. *Biophysical Journal*. 2007;93(4):1255-1263. doi:10.1529/biophysj.106.103192.
123. Wienke D, et al. The collagen receptor Endo180 (CD280) is expressed on basal-like breast tumor cells and promotes tumor growth in vivo. *Cancer Res.* 67:10230-10240, 2007.
124. Wolf K, et al. Multi-step pericellular proteolysis controls the transition from individual to collective cancer cell invasion. *Nat Cell Biol.* 2007;9:893–904.
125. Wolfe JN. Risk for breast cancer development determined by mammographic parenchymal pattern. *Cancer.* 1976;37:2486–92
126. Wozniak MA, Keely PJ. Use of three-dimensional collagen gels to study mechanotransduction in T47D breast epithelial cells. *Biol Proced Online.*; 7:144-161, 2005.
127. Wyckoff J.B., et al. Direct visualization of macrophage-assisted tumor cell intravasation in mammary tumors. *Cancer Res.* 2007;67:2649–56.
128. Xiao Q, Ge G. Lysyl Oxidase, Extracellular matrix remodeling and cancer metastasis. *Cancer Microenviron.* 2012;5:261–73
129. Xu W, et al. Cell stiffness is a biomarker of the metastatic potential of ovarian cancer cells. *PLoS One.* 7:e46609, 2012.
130. Yang X, et al. Chen. Inactivation of lysyl oxidase by β -aminopropionitrile inhibits hypoxia-induced invasion and migration of cervical cancer cells. *Oncol Rep.* 29(2):541-8, 2013.

131. Yamauchi M, Shiiba M. Lysine hydroxylation and cross-linking of collagen. *Methods Mol. Biol.* 2008;446:95–108.
132. Yamauchi M, Sricholpech M. Lysine post-translational modifications of collagen. *Essays Biochem.* 2012;52:113-33.
133. Young JL, Engler AJ. Hydrogels with time-dependent material properties enhance cardiomyocyte differentiation in vitro. *Biomaterials.* 2011;32 (February (4)), 1002–1009.
134. Zaman MH, et al. Migration of tumor cells in 3D matrices is governed by matrix stiffness along with cell-matrix adhesion and proteolysis. *Proc Natl Acad Sci U S A.* 103:10889-10894, 2006.
135. Zhang MH, et al. Estrogen receptor-positive breast cancer molecular signatures and therapeutic potentials (Review). *Biomed reports.* 2014; 2: 41–52.
136. Zhu GG, et al. Immunohistochemical study of type I collagen and type I pN-collagen in benign and malignant ovarian neoplasms. *Cancer.* 1995;75:1010–7.
137. Zhu Y., et al. "Determination of mechanical properties of soft tissue scaffolds by atomic force microscopy nanoindentation." *Journal of biomechanics* 44.13 (2011): 2356-2361.

9. Acknowledgment

There are a number of people to whom I am grateful for their help in the preparation of this thesis.

I would like to acknowledge Dr Emanuele Giordano at the Mol Cell Eng Lab of the Department of Electrical, Electronic and Information Engineering "Guglielmo Marconi" (DEI), Alma Mater Studiorum – University of Bologna for his constructive criticism and helpful comments throughout this study.

A very special thanks to Dr Toni Ibrahim and Dr. Laura Mercatali of the Osteoncology and Rare Tumors Center, Istituto Scientifico Romagnolo per lo Studio e la Cura dei Tumori (IRST) IRCCS, Meldola for their mentorship in conceiving, drafting and planning this work and for the passion in science that every day transmit me.

A genuine thank also to Dr. Alessandro De Vita, Dr. Giacomo Miserocchi, Dr. Chiara Spadazzi, Dr. Ennio Tasciotti, Prof. Luca Cristofolini and Dr. Giovanna Della Porta, for the help in conceiving and realizing all the experimental works of this project and for their constant advices.

I wish to thank also Marco Palanca for his contribution to designing and fine-tuning the compression device.

A very special thanks to Grainne Tierney who edited this work into a perfect English version

Acknowledgements are gratefully made here to the Istituto Scientifico Romagnolo per lo Studio e la Cura dei Tumori (IRST) IRCCS, Meldola, Italy for allowing the opportunity of doing this PhD program.

Lastly, a special mention must be made of my friends and family for their support and encouragement. In particular, I would like to thank my father and my mother without whom my work would never have been possible.

10. List of Publications and Conference Proceedings

Publications

Liverani, C, Mercatali, L, Cristofolini, L et al. Investigating the Mechanobiology of Cancer Cell–ECM Interaction Through Collagen-Based 3D Scaffolds. *Cel. Mol. Bioeng.* (2017) 10: 223.

Liverani C, De Vita A, Minardi S, et al. Biomimetic scaffolds to recreate breast cancer progression and drug resistance (In submission).

Conference Presentation

Liverani, C, Mercatali, L, Cristofolini, L et al. Invasive breast cancer cells are able to increase the stiffness of extracellular collagen. Congress: "Enabling Technologies in 3D Cancer Organoids" (Poster presentation).